Universidade de Aveiro Departamento de Física,
2014

Bruno Alexandre
Zeverino António

Transporte coerente de magnões através de nanoaglomerados magnéticos

Coherent magnon transport through magnetic nanoclusters

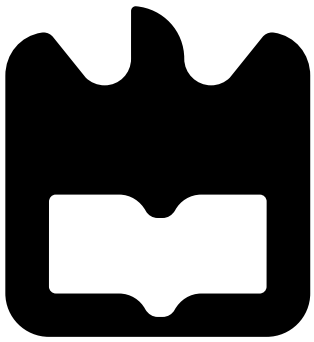

Universidade de Aveiro Departamento de Física,
2014

Bruno Alexandre
Zeverino António

Transporte coerente de magnões através de nanoaglomerados magnéticos

Coherent magnon transport through magnetic nanoclusters

Bruno Alexandre Zeverino António

Transporte coerente de magnões através de nanoaglomerados magnéticos

Coherent magnon transport through magnetic nanoclusters

Dissertação apresentada à Universidade de Aveiro para cumprimento dos requisitos necessários à obtenção do grau de Mestre em Física, realizada sob a orientação científica de Ricardo Dias, Professor do Departamento de Física da Universidade de Aveiro.

o júri / the jury

presidente / president	**Doutor Manuel António dos Santos Barroso** Professor Auxiliar da Universidade de Aveiro
vogais / examiners committee	**Doutor Luís Miguel Fortuna Rodrigues Martelo** Professor Auxiliar da Universidade do Porto
	Doutor Ricardo Assis Guimarães Dias Professor Auxiliar da Universidade de Aveiro (orientador)

agradecimentos / acknowledgements

I would like to express my deep gratitude to Prof. Dr. Ricardo Dias for his valuable guidance.

Resumo

O objetivo principal desta tese é estudar a transmitância de magnões únicos através de nanoaglomerados magnéticos. A nossa abordagem baseia-se na transformação de Matsubara-Matsuda, que mapeia um circuito magnónico de um aglomerado magnético ligado a fios unidimensionais num sistema de bosões *hard-core*. A transmitância de magnões sem interação é calculada através da resolução de um sistema de $N_c + 2$ equações de Schrödinger (onde N_c é o número de sítios do circuito). No caso de magnões com interação foi seguido um método aproximado baseado numa perspectiva de efeito túnel similiar. São discutidos os efeitos na transmitância causados pela interferência quântica dos modos magnónicos, número de coordenação variável no aglomerado e a possibilidade de diferentes magnetizações do aglomerado. É também discutido em detalhe a transmitância de magnões através de clusters magnéticas frustradas.

Abstract

The main goal of this thesis is to study the transmittance of single magnons through magnetic nanoclusters. Our approach relies on the Matsubara-Matsuda transformation, which maps a magnonic circuit of a magnetic cluster connected to 1D leads into a hard-core boson system. The transmittance of non-interacting magnons is computed by solving a system of $N_c + 2$ coupled Schrödinger equations (where N_c is the number of sites of the cluster). In the case of interacting magnons an approximate method was followed which relies in a similar tunnelling perspective. We address the effects in the transmittance of the quantum interference of the magnonic modes, variable coordination number in the cluster, and the possibility of different magnetizations of the nanocluster. Zeeman splitting and anisotropies ($J \neq J^z$) are also addressed but dipole-dipole interactions are not considered. The transmittance of magnons through a frustrated magnetic cluster is discussed.

Contents

List of Figures

Chapter 1

Introduction

A important field within mesoscopic physics is spintronics. Spintronics is expected to become in the near future a potential challenger to the predominance of charge-based electronics.[1, 2] For example, using spin dependent effects one can enhance the storage and processing of data.[3] Futhermore spin waves allow to transmit information without resorting to moving charges with certain technological advantages:

- spin waves can be guided in the magnetic wave-guides (similar to the optical fibres); [4]
- spin wave signal can be converted into a voltage via inductive coupling; [5]
- magnetic field can be used as an external parameter for spin wave signal modulation; [4]
- the absence of moving charges reduces significantly the heat produced by the Joule effect. [1]

Spin waves were not considered as a vehicle for information transmittance for some time due to two disadvantages: relatively slow group velocity (more than two orders of magnitude slower than the speed of light) and high attenuation (more than six orders of magnitude higher attenuation than for photons in a standard optical fibre). These disadvantages are having lower impact than before because, in the deep-submicrometer range, the short travelling distance compensates the slow propagation and high attenuation.[4] Overcoming these disadvantages may allow to use spin waves with wavelength as short as several nano-meters, and with coherence length exceeding tens of micrometers (already produced at room temperature [4]). Efficient coupling to microelectronics poses a vital challenge. Previously developed techniques for spin-wave excitation (spin currents can be produced by spin pumping effect. [2, 6, 7, 8]) may not allow for the relevant downscaling or provide only individual point-like sources.[2, 9]

The observation of spin waves is mainly executed through four methods: inelastic light scattering (such as Brillouin scattering, [10] Raman scattering [11] and inelastic X-ray scattering [12]), inelastic neutron scattering, [13, 14] inelastic electron scattering (spin-resolved electron energy loss spectroscopy), [15] and spin-wave resonance (magnetic resonance). [16, 17] The energy loss of photons reflected from or transmitted through a magnetic material is used in the Brillouin scattering spectroscopy to determine the energy of excited magnons. Although similar to the more widely used Raman scattering it probes lower energies and has a higher energy resolution in order to be able to detect the energy of magnons of the order

of meV. [10] The inelastic neutron scattering method measures the loss of energy of a beam of neutrons due to the excitation of magnons. This energy loss depends on the momentum transfer, temperature and external magnetic field and can be used to determine the dispersion curve for magnons.[13, 14] The same measurement can be achieve by inelastic electron scattering. [15] The absorption of microwaves by spin waves is measured by ferromagnetic or anti-ferromagnetic resonance. This method is suited to determine the effect of magneto-crystalline anisotropy on the dispersion of spin waves. [16, 17]

1.1 Thesis Goals

The main goal of this thesis is the study of the transmittance of magnons through magnetic clusters. Spins in the Heisenberg model can be treated as hard-core bosons through Matsubara-Matsuda transformation. Non-interacting magnons transformed this way map the Heisenberg Hamiltonian into a tight-binding model, which allows to directly compute the transmittance of magnons by solving a system of N_c+2 coupled Schröedinger equations while avoiding quantities such as Green's functions or self energies (where N_c is the number of sites of the cluster). [18] Interacting magnons require the addition of a interacting term in the hard-core boson Hamiltonian. To account for this term of interaction between magnons, a tunnelling perspective was followed. We address the effects in the transmittance of the quantum interference of the magnonic modes, variable coordination number in the cluster, and the possibility of different magnetization of the nanocluster. Zeeman splitting and anisotropies ($J \neq J^z$) are also addressed but dipole-dipole interactions are not considered. This method is used to explore the transmittance through fully ferromagnetic clusters and frustrated magnetic clusters. The contribution of localized magnon states is described.

1.2 Thesis Organization

In chapter 2, three transformations of spin operators into bosonic or fermionic operators are discussed. One of these transformations, the Matsubara-Matsuda transformation, which transforms the Heisenberg Hamiltonian into a hard-core boson Hamiltonian, is used in the following chapters. In chapter 3, the transport of non-interacting magnons through a ferromagnetic cluster is mapped into the transport of single spinless particles described by a tight-binding model. Chapter 4 describes how a tunnelling method can be used to compute the transmittance of interacting magnons on clusters with arbitrary magnetization. A particular frustrated magnetic cluster is studied in chapter 5. Magnetic field induced magnetization and its impact on the overall transmittance of magnons is addressed in chapter 5. Finally, we conclude in chapter 6.

Chapter 2

Heisenberg Magnons

In this chapter, three transformations of spin operators into bosonic or fermionic operators are discussed. This allows to map the problem of the transport of magnons into a problem of the transmittance of fermions or bosons. One of these transformations, the Matsubara-Matsuda transformation, which transforms the Heisenberg Hamiltonian into a hard-core boson Hamiltonian, is used in the following chapters. The Matsubara-Matsuda transformation allows to map the transport of magnons into the transport of bosons while maintaining the simplicity of the Hamiltonian. This is not the case for the Jordan-Wigner transformation where the presence of phase factors makes difficult to obtain analytical results in higher dimensions. Although our study is restricted to particles with spin $S = \frac{1}{2}$, the application of the Holstein-Primakoff transformation for particles with arbitrary spin is discussed. Using this transformation, one could generalize the results of the next chapters for $S \neq \frac{1}{2}$.

2.1 Matsubara-Matsuda transformation

The system to be studied is composed of N interacting fermions with spin 1/2. The interactions between particles are defined by the Heisenberg Hamiltonian that acts on the N particles Hilbert space $\mathcal{H}^N$. The one-particle vector spaces, $|\sigma_i\rangle$, have the standard basis defined as the two possible spin states $|\uparrow\rangle = \begin{pmatrix} 1 \\ 0 \end{pmatrix}$ and $|\downarrow\rangle = \begin{pmatrix} 0 \\ 1 \end{pmatrix}$. The Pauli operators σ_x, σ_y and σ_z are defined in all subspaces $\mathcal{H}_i$ by

$$\sigma^x = \begin{array}{c} \\ \langle\uparrow| \\ \langle\downarrow| \end{array} \begin{array}{c} \begin{array}{cc} |\uparrow\rangle & |\downarrow\rangle \end{array} \\ \begin{pmatrix} 0 & 1 \\ 1 & 0 \end{pmatrix} \end{array}, \tag{2.1}$$

$$\sigma^y = \begin{array}{c} \\ \langle\uparrow| \\ \langle\downarrow| \end{array} \begin{array}{c} \begin{array}{cc} |\uparrow\rangle & |\downarrow\rangle \end{array} \\ \begin{pmatrix} 0 & -i \\ i & 0 \end{pmatrix} \end{array}, \tag{2.2}$$

$$\sigma^z = \begin{array}{c} \\ \langle\uparrow| \\ \langle\downarrow| \end{array} \begin{array}{c} \begin{array}{cc} |\uparrow\rangle & |\downarrow\rangle \end{array} \\ \begin{pmatrix} 1 & 0 \\ 0 & -1 \end{pmatrix} \end{array}. \tag{2.3}$$

$$\tag{2.4}$$

These operators satisfy the same commuting algebra as the spin operators

$$[\sigma^a, \sigma^b] = i\epsilon_{abc}\sigma^c, \text{ for } a, b, c \in \{x, y, z\}. \tag{2.5}$$

When Pauli operators operate in different subspaces, they are independent and commute. They also satisfy an anti-commuting algebra

$$\{\sigma^a, \sigma^b\} = \frac{1}{2}\delta_{ab}, \text{ for } a, b, c \in \{x, y, z\}. \tag{2.6}$$

One may define the ladder operators σ^+ and σ^- in all subspaces $|\sigma_i\rangle$ by

$$\sigma^+ = \begin{array}{c} \\ \langle\uparrow| \\ \langle\downarrow| \end{array} \begin{array}{c} \begin{array}{cc} |\uparrow\rangle & |\downarrow\rangle \end{array} \\ \begin{pmatrix} 0 & 2 \\ 0 & 0 \end{pmatrix} \end{array}, \tag{2.7}$$

$$\sigma^- = \begin{array}{c} \\ \langle\uparrow| \\ \langle\downarrow| \end{array} \begin{array}{c} \begin{array}{cc} |\uparrow\rangle & |\downarrow\rangle \end{array} \\ \begin{pmatrix} 0 & 0 \\ 2 & 0 \end{pmatrix} \end{array}. \tag{2.8}$$

$$\tag{2.9}$$

The commutation relation between σ^+ and σ^- is

$$\left[\sigma^+, \sigma^-\right] = 2\sigma^z. \tag{2.10}$$

The Pauli operators can be rewritten as

$$\sigma^x = \frac{1}{2}\left(\sigma^+ + \sigma^-\right), \tag{2.11}$$

$$\sigma^y = \frac{1}{2i}\left(\sigma^+ - \sigma^-\right). \tag{2.12}$$

$$\tag{2.13}$$

The spin operators are written at the expense of the Pauli matrices (with $\hbar = 1$)

$$S^z = \frac{1}{2}\sigma^x \quad ; \quad S^y = \frac{1}{2}\sigma^y \quad ; \quad S^z = \frac{1}{2}\sigma^z \quad ; \quad S^+ = \frac{1}{2}\sigma^+ \quad ; \quad S^- = \frac{1}{2}\sigma^- \tag{2.14}$$

The generalized Heisenberg model Hamiltonian operates in the space $\mathcal{H}^N$ and it is described as

$$H = -\sum_{\langle i,j \rangle} J^x_{i,j} S^x_i S^x_j + J^y_{i,j} S^y_i S^y_j + J^z_{i,j} S^z_i S^z_j + h \sum_j S^z_j, \tag{2.15}$$

where $J^x_{i,j}$, $J^y_{i,j}$ and $J^z_{i,j}$ are the x, y and z components of the Heisenberg coupling, h is the energy associated with an externally applied magnetic field and $\langle i,j \rangle$ represents all pairs of nearest neighbours. Considering isotropy in the XY plane, i.e. $J^x_{i,j} = J^y_{i,j} = J_{i,j}$, the Hamiltonian can be written as

$$H = -\sum_{\langle i,j \rangle} J_{i,j} \left(S^x_i S^x_j + S^y_i S^y_j \right) - \sum_{\langle i,j \rangle} J^z_{i,j} S^z_i S^z_j + h \sum_j S^z_j. \tag{2.16}$$

Replacing S^x and S^y by S^+ and S^-,the previous equation becomes

$$H = -\sum_{\langle i,j \rangle} \frac{J_{i,j}}{2} \left(S^+_i S^-_j + S^+_j S^-_i \right) - \sum_{\langle i,j \rangle} J^z_{i,j} S^z_i S^z_j + h \sum_j S^z_j. \tag{2.17}$$

Spin operators associated with magnons are difficult to deal with, as spins operators do not respect the bosonic nor the fermionic commutation rules.[19] It is required to transform these spins operators into more handleable operators in order to perform analytic and computational operations. The Matsubara-Matsuda transformation is used to obtain a spinless hard-core boson Hamiltonian which, in the presence of a single magnon, becomes a tight-binding Hamiltonian.

The Matsubara-Matsuda transformation replaces the spin operators of particles with spin 1/2 with bosonic creation and annihilation operators for any given geometry.[20] Normally bosonic distributions allow to have more than a particle per state. This is not compatible with the "fermionic" distribution of magnons. This incompatibility, however, can be surpassed if one considers that it is possible to have two or more bosons in the same state, but the respective required energy is infinite. This way we have a group of particles whose creation and annihilation operators respect the bosonic commutation rules and respect the fermionic distribution. These particles are called hard-core bosons. The transformation can be expressed as

$$\begin{cases} S^+_j = b^\dagger_j, \\ S^-_j = b_j, \\ S^z_j = b^+_j b_j - \frac{1}{2} = n_j - \frac{1}{2}, \end{cases} \tag{2.18}$$

where S^+_j, S^-_j and S^z_j are the spin raising, lowering and z component operators and $b^\dagger_j$, b_j and n_j are the boson creation, annihilation and occupation operators, respectively. These operators respect the boson commutation relations, but with a hard-core condition,

$$[b_i, b^+_j] = \delta_{ij} \left(1 - 2 b^\dagger_i b_j \right); \quad [b^\dagger_i, b^\dagger_j] = 0. \tag{2.19}$$

With this transformation, one can transform an Heisenberg model Hamiltonian

$$H = -\sum_{\langle i,j\rangle} \frac{J_{i,j}}{2}\left(S_i^+ S_j^- + S_j^+ S_i^-\right) - \sum_{\langle i,j\rangle} J_{i,j}^z S_i^z S_j^z + h\sum_j S_j^z \tag{2.20}$$

into a spinless hard-core boson Hamiltonian

$$H = -\sum_{\langle i,j\rangle} \frac{J_{i,j}}{2}\left(b_i^\dagger b_j + b_j^\dagger b_i\right) - \sum_{\langle i,j\rangle} J_{i,j}^z \left(n_i - \frac{1}{2}\right)\left(n_j - \frac{1}{2}\right) + h\sum_j \left(n_j - \frac{1}{2}\right). \tag{2.21}$$

The previous transformation can be applied to a 1D uniform chain which gives

$$H = -J/2\sum_j \left(b_{j+1}^\dagger b_j + b_j^\dagger b_{j+1}\right) + J^z\sum_j n_j - J^z\sum_j n_j n_{j+1} + h\sum_j \left(n_j - \frac{1}{2}\right). \tag{2.22}$$

2.2 Jordan-Wigner transformation

The Jordan-Wigner transformation turns spin operators into fermionic operators.[21, 22] In order for these fermionic operators to respect the commutation and anti-commutation rules of the spin operators, phase factors must be added. In this section, the Jordan-Wigner transformation is performed in the case of a 1D chain to obtain the one-magnon energy dispersion. Note that for one magnon the Jordan-Wigner transformation is equivalent to the Matsubara-Matsuda transformation. The Jordan-Wigner transformation is then executed in a 2D square lattice to show that the transformation depends on the geometry of the system and its level of complexity increases rapidly with increasing dimensionality. This presents an issue for the implementation of the Jordan-Wigner transformation to clusters with arbitrary geometries.

2.2.1 Jordan-Wigner transformation in 1D chains

Jordan and Wigner [23] realized that the down and up state of a single spin can be viewed of as an empty or singly occupied fermion state

$$|\downarrow\rangle \equiv |0\rangle \quad \text{and} \quad |\uparrow\rangle \equiv f^\dagger|0\rangle \equiv |1\rangle\,. \tag{2.23}$$

An explicit representation of the spin operators in terms of fermion operators is then

$$\hat{S}^+ = f^\dagger = \begin{matrix} \\ \langle 1| \\ \langle 0| \end{matrix}\begin{matrix} \begin{matrix} |1\rangle & |0\rangle \end{matrix} \\ \begin{pmatrix} 0 & 1 \\ 0 & 0 \end{pmatrix} \end{matrix}, \tag{2.24}$$

$$\hat{S}^- = f = \begin{matrix} \\ \langle 1| \\ \langle 0| \end{matrix}\begin{matrix} \begin{matrix} |1\rangle & |0\rangle \end{matrix} \\ \begin{pmatrix} 0 & 0 \\ 1 & 0 \end{pmatrix} \end{matrix}, \tag{2.25}$$

$$\hat{S}^z = \frac{1}{2}\begin{matrix} \\ \langle 1| \\ \langle 0| \end{matrix}\begin{matrix} \begin{matrix} |1\rangle & |0\rangle \end{matrix} \\ \begin{pmatrix} 1 & 0 \\ 0 & -1 \end{pmatrix} \end{matrix}, \tag{2.26}$$

$$\tag{2.27}$$

This way, the Pauli spin operators provided Jordan and Wigner with an elementary model of a fermion. This representation needs to be modified when there is more than one spin, as independent spin operators commute but independent fermions anticommute. This was fixed in 1D by attaching a phase factor called a "string" to the fermionic operators. [23] For a 1D chain of spins, the Jordan-Wigner representation of the spin operator at site j is defined as

$$S_j{}^+ = f_j{}^\dagger e^{i\phi_j}, \tag{2.28}$$

where the phase operator ϕ_j contains the sum over all fermion occupancies at sites to the left of j,

$$\phi_j = \pi \sum_{w<j} f_w{}^\dagger f_w = \pi \sum_{w<j} n_w, \tag{2.29}$$

where n_w represents the fermionic occupation operator. The complete Jordan-Wigner transformation is then

$$\begin{cases} S_j{}^z = f^+ f - \dfrac{1}{2}, \\ S_j{}^+ = f_j^\dagger e^{i\pi \sum_{w<j} n_w}, \\ S_j{}^- = f_j e^{-i\pi \sum_{w<j} n_w}. \end{cases} \tag{2.30}$$

Now these fermionic operators obey to the fermionic anti-commutations rules

$$\{f_i^\dagger, f_j\} = \delta_{ij}, \quad \text{and} \quad \{f_i^\dagger, f_j^\dagger\} = 0. \tag{2.31}$$

The important point in this representation is that the operator $e^{i\pi n_j}$ anticommutes with the fermion operators at the same site:

$$\{e^{i\pi n_j}, f_j{}^\dagger\} = e^{i\pi n_j} f_j{}^\dagger + f_j{}^\dagger e^{i\pi n_j} = e^{i\pi n_j} \left(f_j{}^\dagger - f_j{}^\dagger \right) = 0. \tag{2.32}$$

The transverse spin operators now satisfy the correct commutation algebra. The following relations are also satisfied:

$$[e^{i\pi\phi_k}, f_j] = \begin{cases} 0, & j \geq k, \\ 2\exp\left(i\pi \sum\limits_{\substack{w<k \\ w\neq j}} n_w \right), & j < k. \end{cases} \tag{2.33}$$

To see how this works, we shall now discuss the one-dimensional Heisenberg model in the absence of an applied external magnetic field (i.e. $h = 0$)

$$H = -J \sum_j [S_j^x S_{j+1}^x + S_j^y S_{j+1}^y] - J^z \sum_j S_j^z S_{j+1}^z \tag{2.34}$$

$$= -\frac{J}{2} \sum_j [S_{j+1}^+ S_j^- + H.C.] - J^z \sum_j S_j^z S_{j+1}^z. \tag{2.35}$$

To fermionize the first term, we note that all terms in the string cancel, except for a $e^{i\pi n_j}$ which has no effect,

$$\frac{J}{2} \sum_j S_{j+1}^+ S_j^- = \frac{J}{2} \sum_j f_{j+1}^\dagger e^{i\pi n_j} f_j = \frac{J}{2} \sum_j f_{j+1}^\dagger f_j. \tag{2.36}$$

The z-component of the Hamiltonian becomes

$$-J^z \sum_j S^z_{j+1} S^z_j = -J^z \sum_j \left(n_{j+1} - \frac{1}{2}\right)\left(n_j - \frac{1}{2}\right). \tag{2.37}$$

The transformed Hamiltonian is then (ignoring the constant term):

$$H = -\frac{J}{2} \sum_j \left(f^\dagger_{j+1} f_j + f^\dagger_j f_{j+1}\right) + J^z \sum_j n_j - J^z \sum_j n_j n_{j+1}. \tag{2.38}$$

A more compacted expression can be achieved by transforming it to the momentum space. The resulting Hamiltonian is deduced in the appendix A and can be written as

$$H = \sum_k \omega_k f^\dagger_k f_k - \frac{J^z}{N} \sum_{k,k',q} \cos(qa) f^\dagger_{k-q} f^\dagger_{k'+q} f_{k'} f_k, \tag{2.39}$$

where $\omega_k = (J^z - J\cos ka)$ is the one-magnon excitation energy. If one neglects the interactions in the case when $J^z = J > 0$, the spectrum

$$\omega_k = (J - J\cos ka) = 2J\sin^2(ka/2) \tag{2.40}$$

is always positive so that there are no magnons present in the ground-state as it more energetic then a pure ferromagnetic state. The ground state can be written as

$$|\Psi_g\rangle = |\mathrm{Fe}(\downarrow)\rangle = |\downarrow\downarrow\downarrow ...\rangle \tag{2.41}$$

which corresponds to a state with a spontaneous magnetization $M = \sum_j S^z_j |\Psi_g\rangle = -N/2$. Since $\omega_{k=0} = 0$, it costs no energy to add a magnon of arbitrarily long wavelength. This is an example of a Goldstone mode, where the spontaneous magnetization can point in any direction perpendicular to the chain axis. Rotating the magnetization should cost no energy, and this is the reason why the $k = 0$ magnon is a zero energy excitation. When $J^z = 0$ and $J > 0$, the spectrum becomes $\omega_k = -J\cos ka$ and magnon states with negative energy will become occupied. All the negative energy fermion states with $|k| < \pi/2a$ are occupied, so the ground-state is given by

$$|\Psi_g\rangle = \prod_{|k|<\frac{\pi}{2a}} f^\dagger_k |0\rangle. \tag{2.42}$$

The band of magnon states is thus precisely half-filled,

$$\langle S^z\rangle = \langle n_f - \frac{1}{2}\rangle = 0, \tag{2.43}$$

so that remarkably, there is no ground-state magnetization. The ground state energy is given by (see appendix B)

$$E_g = -J \sum_{|k|<\pi/2a} |\cos(ka)| = \frac{-JN}{\pi}. \tag{2.44}$$

An excitation can be produced by adding a magnon with wavevector $|k| > \pi/2a$ or by annihilating a magnon with $|k| < \pi/2a$, thus creating a hole.

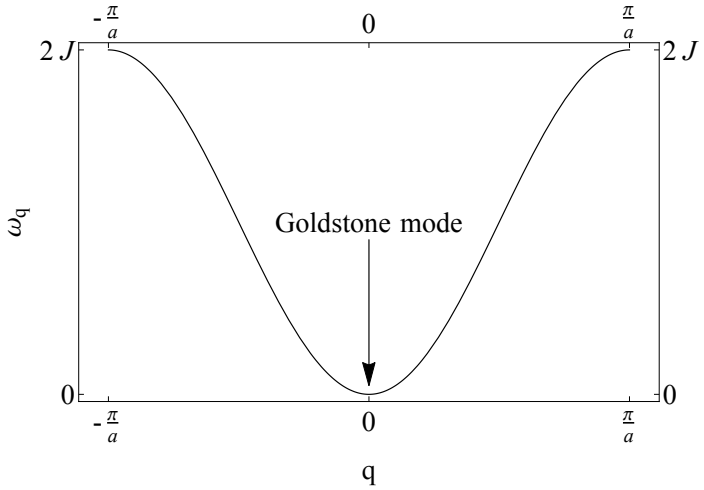

Figure 2.1: One-magnon excitation spectrum of the one-dimensional ($J^z = J > 0$) Heisenberg ferromagnet in the absence of magnetic field ($h = 0$). The ferromagnetic nature of the ground state implies a rotational symmetry which is broken by a Goldstone boson.

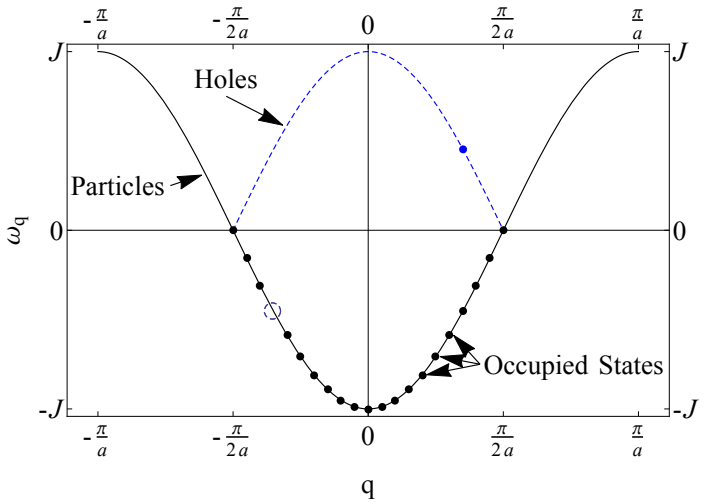

Figure 2.2: One-magnon excitation spectrum of the one dimensional ($J^z = 0$ and $J > 0$) Heisenberg ferromagnet in the absence of magnetic field ($h = 0$). The ground state is the state with the negative energy positions occupied by magnons. The annihilation of a magnon on the ground state is equivalent to create a hole with opposite energy and momentum.

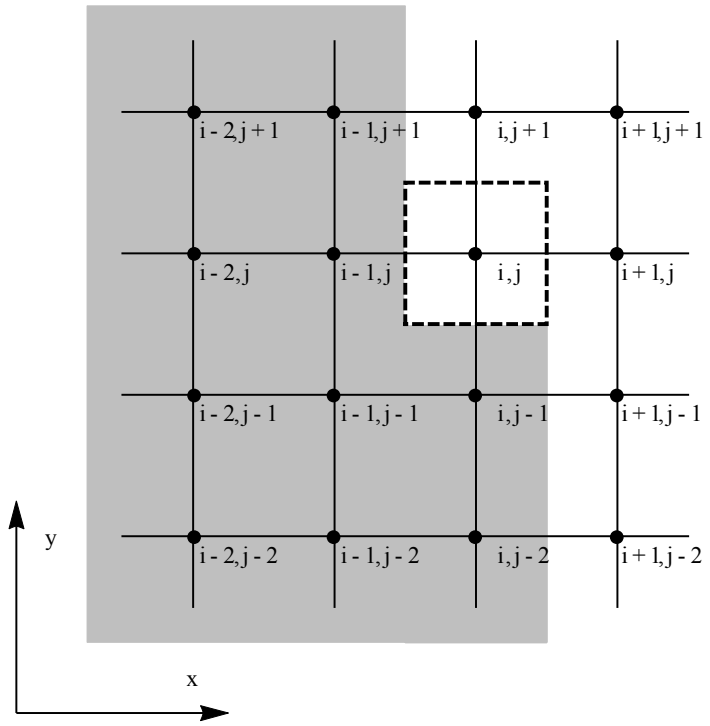

Figure 2.3: Schematic representation of the order of the indexes. The phase of the fermionic operators on the site i, j depends on the total occupation in the grey area.

2.2.2 Jordan-Wigner in two dimensions

In chapter 3 and 4, we consider the Heisenberg Hamiltonian for nanoclusters of arbitrary geometry. The Jordan-Wigner transformation for a system of 1D leads connected to this nanocluster is rather more complicated.

The square lattice allows to analytically express a transformed Hamiltonian and demonstrate the increasing difficulty in using the Jordan-Wigner transformation.[21, 24] The extended Jordan-Wigner transformation for a 2D square lattice can be defined as

$$s^-_{i,j} = f_{i,j} e^{i\alpha_{i,j}} \tag{2.45}$$

$$= e^{i\alpha_{i,j}} f_{i,j}, \tag{2.46}$$

$$s^+_{i,j} = f^\dagger_{i,j} e^{-i\alpha_{i,j}} \tag{2.47}$$

$$= e^{-i\alpha_{i,j}} f^\dagger_{i,j}, \tag{2.48}$$

$$\alpha_{i,j} = \pi \left(\sum_{d=0}^{i-1} \sum_{f=0}^{\infty} n_{d,f} + \sum_{f=0}^{j-1} n_{i,f} \right), \tag{2.49}$$

where $n_{d,f} = f^\dagger_{d,f} f_{d,f}$. The first term sums for all the columns on the left while the second term sum on the i column until the $i, j-1$. One can use the Jordan-Wigner transformation

to rewrite the Hamiltonian (see appendix C)

$$H = \underbrace{\sum_{i=0}^{\infty}\sum_{j=0}^{\infty} J\left(\mathbf{S}_{i,j}\mathbf{S}_{i+1,j} + \mathbf{S}_{i,j}\mathbf{S}_{i,j+1}\right)}_{H_{xyz}} + \underbrace{\sum_{i=0}^{\infty}\sum_{j=0}^{\infty} hS_{i,j}^{z}}_{H_{Zeeman}} \tag{2.50}$$

as the sum of the components

$$\begin{aligned} H_{xy} = \frac{1}{2}\sum_{i=0}^{\infty}\sum_{j=0}^{\infty} & J_{i,j,i+1,j}\left(-f_{i,j}e^{i\tilde{\phi}_{i,i+1}(j)}f_{i+1,j}^{\dagger} + f_{i,j}^{\dagger}e^{-i\tilde{\phi}_{i,i+1}(j)}f_{i+1,j}\right) \\ & + J_{i,j,i,j+1}\left(-f_{i,j}f_{i,j+1}^{\dagger} + f_{i,j}^{\dagger}f_{i,j+1}\right), \end{aligned} \tag{2.51}$$

$$\begin{aligned} H_{z} = \sum_{i=0}^{\infty}\sum_{j=0}^{\infty} & J_{i,j,i+1,j}\left(f_{i,j}^{\dagger}f_{i,j} - \frac{1}{2}\right)\left(f_{i+1,j}^{\dagger}f_{i+1,j} - \frac{1}{2}\right) \\ & + J_{i,j,i,j+1}\left(f_{i,j}^{\dagger}f_{i,j} - \frac{1}{2}\right)\left(f_{i,j+1}^{\dagger}f_{i,j+1} - \frac{1}{2}\right) \end{aligned} \tag{2.52}$$

and

$$\begin{aligned} H_{Zeeman} &= \sum_{i=0}^{\infty}\sum_{j=0}^{\infty} h\left(s_{i,j}^{+}s_{i,j}^{-} - \frac{1}{2}\right) \\ &= \sum_{i=0}^{\infty}\sum_{j=0}^{\infty} h\left(f_{i,j}^{\dagger}f_{i,j} - \frac{1}{2}\right), \end{aligned} \tag{2.53}$$

where $\tilde{\phi}_{i,i+1}(j) = \pi\left(\sum_{w=j+1}^{\infty} n_{i,w} + \sum_{w=0}^{j-1} n_{i+1,w}\right)$.

2.2.3 One particle Jordan-Wigner transformation

The Jordan-Wigner transformation introduces phases that depend on the distribution of the fermions in the lattice. The operators present in Heisenberg Hamiltonian produce pairs of annihilation and creation operators that act at the same site or at nearest neighbours. The presence of multiple particles and generalized connections between sites results in a Jordan-Wigner Hamiltonian which can be seen as a tight-binding model as in the case of the Matsubara-Matsuda Hamiltonian but the hopping constants contain phases which have a different expression every time any particle changes position. This does not happen with the Matsubara-Matsuda Hamiltonian except when there is a single magnon in the structure. The Jordan-Wigner Hamiltonian only acts at the particle's site and at the sites that it connects to. Other sites have zero contribution because the annihilation operators will operate at empty sites. Consider the generalized situation presented in figure 2.4. The position index used in the phases summation runs from left to right. The Hamiltonian terms that require attention are $S_b^+S_a^- + S_a^+S_b^-$ and $S_c^+S_b^- + S_b^+S_c^-$:

$$S_b^+S_a^- + S_a^+S_b^- \implies f_b^{\dagger}e^{i\pi\sum_{j\geq a}^{b-1} n_j}f_a + f_a^{\dagger}e^{-i\pi\sum_{j\geq a}^{b-1} n_j}f_b \overset{N=1}{\Longrightarrow} f_a^{\dagger}f_b + f_b^{\dagger}f_a \tag{2.54}$$

$$S_c^+S_b^- + S_b^+S_c^- \implies f_c^{\dagger}e^{i\pi\sum_{j\geq b}^{c-1} n_j}f_b + f_b^{\dagger}e^{-i\pi\sum_{j\geq b}^{c-1} n_j}f_c \overset{N=1}{\Longrightarrow} f_c^{\dagger}f_b + f_b^{\dagger}f_c \tag{2.55}$$

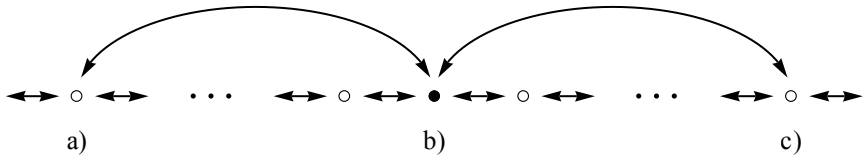

Figure 2.4: Schematic representation of a tight binding model with generalized connections. Points a) and c) can be any site with lower or higher position index than the site b).

---

which are equivalent to the Matsubara-Matsuda transformation when only a particle is present. Even though the Jordan-Wigner transformation is, in essence, different from the Matsubara-Matsuda transformation, the terms that distinguish between transformations cancel in the case of a single particle. This way, the physical properties deduced for an one-dimensional lead occupied with a single fermion are valid for an one-dimensional lead occupied with a single hard-core boson.

2.3 Holstein-Primakoff transformation

The Holstein-Primakoff transformation allows to express the spin operators of particles with arbitrary spin as boson operators.[25, 26] It is best suited when the particles to be transformed have large spins. The usage of the Holstein-Primakoff transformation for particles with spin 1/2 adds complexity, while it does not present any advantage over the Matsubara-Matsuda transformation. Although the Holstein-Primakoff transformation can be executed for an anisotropic anti-ferromagnetic structure, here focus is given to the isotropic ferromagnetic case, i.e. $J_{i,j} = J > 0$. The Hamiltonian in equation 2.20 can then be written as

$$H = -J \sum_{\mathbf{j},\boldsymbol{\delta}} \mathbf{S_j} \cdot \mathbf{S_{j+\delta}} - 2\mu_0 H_0 \sum_{\mathbf{j}} S^z_{\mathbf{j}}, \tag{2.56}$$

where the vectors $\boldsymbol{\delta}$ connect atom $\mathbf{j}$ with its nearest neighbors, $\mu_0 = (g/2)\mu_B$ is the magnetic moment, $\mathbf{S_j}$ is the spin operator at site $\mathbf{j}$, H_0 is the intensity of a static magnetic field directed along the z axis with associated energy of $h = 2\mu_0 H_0$. H_0 is chosen to be positive in order to make the spins align along the positive z axis when the system is in the ground state. The Holstein-Primakoff transformation enables to express the spin operators as boson creation and annihilation operators $a^\dagger_{\mathbf{j}}$ and $a_{\mathbf{j}}$, respectively:

$$S^+_{\mathbf{j}} = S^x_{\mathbf{j}} + iS^y_{\mathbf{j}} = (2S)^{1/2}(1 - a^\dagger_{\mathbf{j}} a_{\mathbf{j}}/2S)^{1/2} a_{\mathbf{j}} \tag{2.57}$$

$$S^-_{\mathbf{j}} = S^x_{\mathbf{j}} - iS^y_{\mathbf{j}} = (2S)^{1/2} a^\dagger_{\mathbf{j}} (1 - a^\dagger_{\mathbf{j}} a_{\mathbf{j}}/2S)^{1/2}. \tag{2.58}$$

The maximum bosonic occupation is limited by $2S$. While it is possible to have states with more than $2S$ bosons, these states do not have physical meaning. This restriction is lifted when $S \to \infty$. It is required that S^+ and S^- satisfy the correct commutation relations, which

means that

$$[a_{\mathbf{j}}, a^{\dagger}_{\mathbf{w}}] = \delta_{\mathbf{jw}} \tag{2.59}$$

must be satisfied. The transformation of S^+,S^- and S^z turns the Hamiltonian

$$H = -J \sum_{\mathbf{j},\boldsymbol{\delta}} \mathbf{S}_{\mathbf{j}} \cdot \mathbf{S}_{\mathbf{j}+\boldsymbol{\delta}} - 2\mu_0 H_0 \sum_{\mathbf{j}} S^z_{\mathbf{j}} \tag{2.60}$$

into a Hamiltonian, considering z nearest neighbours,

$$H = -JNzS^2 - 2\mu_0 H_0 NS + \mathbb{H}_0 + \mathbb{H}_1. \tag{2.61}$$

The first two terms have order zero while $\mathbb{H}_0$ has the second order components and $\mathbb{H}_1$ has the terms with higher order. The bilinear term in spin-wave variables is given by

$$\begin{aligned} \mathbb{H}_0 = -JS/N \sum_{\mathbf{j},\boldsymbol{\delta},\mathbf{k},\mathbf{k}'} \Big(& e^{-i(\mathbf{k}-\mathbf{k}')\cdot\mathbf{x}_{\mathbf{j}}} e^{i\mathbf{k}\cdot\boldsymbol{\delta}} b_{\mathbf{k}} b^{\dagger}_{\mathbf{k}'} + e^{i(\mathbf{k}-\mathbf{k}')\cdot\mathbf{x}_{\mathbf{j}}} e^{-i\mathbf{k}'\cdot\boldsymbol{\delta}} b^{\dagger}_{\mathbf{k}} b_{\mathbf{k}'} \\ & - e^{i(\mathbf{k}-\mathbf{k}')\cdot\mathbf{x}_{\mathbf{j}}} b^{\dagger}_{\mathbf{k}} b_{\mathbf{k}'} - e^{-i(\mathbf{k}-\mathbf{k}')\cdot(\mathbf{x}_{\mathbf{j}}+\boldsymbol{\delta})} b^{\dagger}_{\mathbf{k}} b_{\mathbf{k}'} \Big) \\ & + 2\mu_0 h/N \sum_{\mathbf{j},\mathbf{k},\mathbf{k}'} e^{i(\mathbf{k}-\mathbf{k}')\cdot\mathbf{x}_{\mathbf{j}}} b^{\dagger}_{\mathbf{k}} b_{\mathbf{k}'}. \end{aligned} \tag{2.62}$$

For sc, bcc and fcc lattices of lattice constant a, the exchange contribution to the magnon frequency has the form of the de Broglie dispersion relation for a free particle of mass m^*:

$$\omega_{\mathbf{k}} = 2\mu_0 H_0 + 2JS(\mathbf{k}a)^2, \tag{2.63}$$

where $2JSa^2 = 1/(2m^*)$ or $m^* = 1/4JSa^2$

Chapter 3

Transport through ferromagnetic clusters

In this chapter, the transmittance of a single magnon through a ferromagnetic cluster connected by ferromagnetic leads is addressed.

In ferromagnetic clusters, if only one spin is inverted at any given time, this implies that there is only a magnon present in the system. This magnon can be produced by parallel pumping outside of the cluster and for simplicity, we assume it is directed to the cluster by a one-dimensional chain (left lead) and then leaves the cluster by another one-dimensional chain (right lead) with a probability that reflects the properties of the cluster (see figure 3.1).

This chapter is organized in the following way. Firstly the existence of local potential generated by the geometry of the system is addressed. Then the XY limit and anisotropic cases are compared to the tight-binding model. The followed approach to compute the transmittance of a single magnon through a ferromagnetic cluster is described. The approach is used for a 8 sites perfect ring and a Fe_7 structure and the physical interpretation of the results is exposed. Lastly the effects of the presence of a magnetic tip are explored as a method of wavefunctions imaging.

3.1 Topological effects in clusters

In principle, the transmittance of a single magnon through a ferromagnetic system should be the same as that of a single spinless particle through the equivalent tight-binding model. However, an interesting effect can be seen when expanding the middle term of the equation 2.21:

$$\begin{aligned} -\sum_{\langle i,j\rangle} J^z_{i,j}\left(b^\dagger_i b_i-\frac{1}{2}\right)\left(b^\dagger_j b_j-\frac{1}{2}\right) &= -\sum_{\langle i,j\rangle} J^z_{i,j}\left(b^\dagger_i b_i b^\dagger_j b_j-\frac{1}{2}b^\dagger_i b_i-\frac{1}{2}b^\dagger_j b_j+\frac{1}{4}\right)= \\ &= -\sum_{\langle i,j\rangle} J^z_{i,j}\left(n_i n_j-\frac{1}{2}n_i-\frac{1}{2}n_j+\frac{1}{4}\right). \end{aligned} \tag{3.1}$$

Considering $J^z_{i,j}$ to be site independent, [23]

$$-J^z\sum_{\langle i,j\rangle}-\frac{1}{2}n_i-\frac{1}{2}n_j=-J^z\sum_{\langle i,j\rangle}-n_i=\frac{J^z}{2}\sum_j Z_j n_j, \tag{3.2}$$

with Z_i being the coordination number of the site i, equation 3.1 becomes

$$-J^z \sum_{\langle i,j \rangle} n_i n_j + \frac{J^z}{2} \sum_j Z_j n_j - J^z \sum_{\langle i,j \rangle} \frac{1}{4}. \tag{3.3}$$

The first term of equation 3.3 is different of zero only when there are at least two magnons at nearest neighbours sites. For now, this term is zero due to the presence of a single magnon. The third term of 3.3 is a particular constant for each cluster. The remaining term reveals that the onsite energy of a magnon at a particular site changes with the number of neighbour sites. This is a interesting result as in the standard tight-binding no local potential generated by the geometry of the system is considered.

3.2 The XY limit, $J^z = 0$

The hard-core boson Hamiltonian for $J^z = 0$ is given by equation 2.21. Note that $J^z = 0$ usually implies that the system is paramagnetic and the spin direction is arbitrary. Here, however, we may assume the spins' direction is externally defined by an uniform magnetic field. The existence of an external local magnetic field in the cluster region is also considered. This local magnetic field could be produced by a magnetic probe whose position influences the overall transmittance of magnons. The hard-core boson Hamiltonian with $J^z = 0$ and a local magnetic field in the cluster, h_j, is given by

$$H = -\sum_{\langle i,j \rangle} \frac{J_{i,j}}{2} \left(b_i^\dagger b_j + b_j^\dagger b_i \right) + \sum_j h_j \left(n_j - \frac{1}{2} \right), \tag{3.4}$$

As there is a single incoming magnon from the left lead, we only need to consider a single inverted spin, that is, states of the form

$$|j\rangle = b_j^\dagger \left| \mathrm{Fe}(\downarrow) \right\rangle, \tag{3.5}$$

where $|\mathrm{Fe}(\downarrow)\rangle$ represents the state with all spins down (which is the vacuum of the hard-core bosons). The energy term associated with the uniform magnetic field is dropped since it is a constant and therefore it will not affect the transmittance. This allows the hard-core Hamiltonian to be treated as a spinless one particle tight-binding Hamiltonian (and drop the second quantization notation). One can map the Heisenberg coupling, $J/2$, to the tight-binding hopping constant, t and the local magnetic field intensity h_j to the on-site energy, ϵ_j. This tight-binding approach can be directly used to compute the cluster eigenstates and the transmittance of non-interacting magnons.

The Hamiltonian of the system is the sum of the leads and cluster Hamiltonians, H_0, and the coupling between each lead and the cluster, V_{LR},

$$H = H_0 + V_{LR}, \tag{3.6}$$

with

$$H_0 = \underbrace{-\sum_{j=-\infty}^{0} \left(|j-1\rangle\langle j| + \mathrm{H.c.} \right)}_{\text{Left lead}} \underbrace{-\sum_{j=N+1}^{\infty} \left(|j\rangle\langle j+1| + \mathrm{H.c.} \right)}_{\text{Right lead}} + \underbrace{H_c}_{\text{cluster}} \tag{3.7}$$

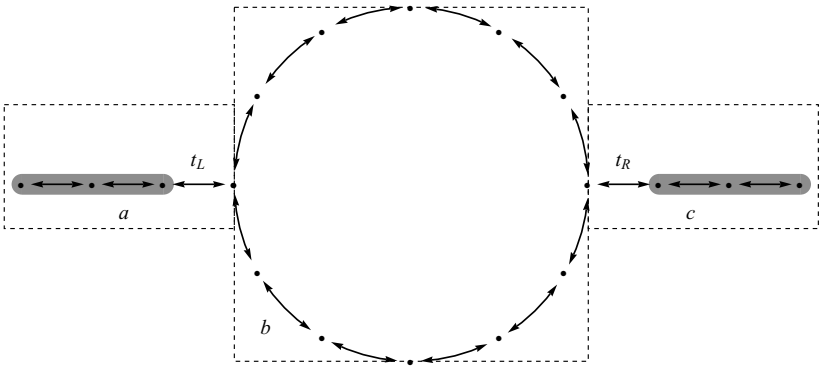

Figure 3.1: Schematic representation of the studied systems. In (a) and (c) one has the left and right semi-infinite 1D leads, respectively. These leads are considered to be perfect conductors. In (b), we show the cluster described by a tight-binding model. For simplification purposes it is represented by a ring. The hopping factors which couple the left and right leads to the cluster are, respectively, t_L and t_R.

---

where H_c is the single-magnon Hamiltonian in the scattering region (the cluster). The leads connected to the cluster are considered ideal (we assume $J/2 = t = 1$). The coupling V_{LR} between the leads and the cluster is given by

$$V_{LR} = -t_L|0\rangle\langle 1| - t_R|N\rangle\langle N+1| + \text{H.c.}, \tag{3.8}$$

where the hopping matrix elements t_L e t_R connect the left and right leads, respectively, to the cluster and result from the Heisenberg coupling $J_L/2 = t_L$ and $J_R/2 = t_R$ (we assume that these coupling may be different from the couplings in the cluster and in the leads). The Hamiltonian of the cluster is

$$H_c = -\sum_{\langle i,j\rangle}(t_{ij}|i\rangle\langle j| + \text{H.c.}) + \sum_j \epsilon_j|j\rangle\langle j| - \frac{1}{2}\left(\sum_j \epsilon_j\right)\hat{\mathbb{I}}, \tag{3.9}$$

where ϵ_j is the on-site energy, t_{ij} is the hopping integral between two nearest neighbour sites and $\hat{\mathbb{I}} = \sum_j |j\rangle\langle j|$ is the identity operator in the cluster subspace. Note that despite the fact that $-\frac{1}{2}\left(\sum_j \epsilon_j\right)\hat{\mathbb{I}}$ is a constant for a given set of $\{\epsilon_1, \epsilon_2, \epsilon_3, ...\}$, its value depends on the values of all on-site energies. For this reason it cannot be neglected, as seen in section 3.7.

3.3 The anisotropic case, $J^z \neq 0$

We now consider the hard-core Hamiltonian with $J^z \neq 0$ and a local magnetic field. The spins remain aligned and there is only a single incoming magnon from the left lead. The previous assumptions are valid and although the hard-core Hamiltonian is slightly different,

it can be described as a tight-binding Hamiltonian with interactions:

$$H = -\sum_{\langle i,j\rangle} \frac{J_{i,j}}{2}\left(b_i^\dagger b_j + b_j^\dagger b_i\right) - \sum_{\langle i,j\rangle} J_{i,j}^z n_i n_j + \frac{1}{2}\sum_{\langle i,j\rangle} J_{i,j}^z n_j - \sum_{\langle i,j\rangle} \frac{J_{i,j}^z}{4} + \sum_j h_j\left(n_j - \frac{1}{2}\right). \quad (3.10)$$

As seen previously, in the case of single magnon, this Hamiltonian can be reduced to (dropping the constant terms)

$$H = -\sum_{\langle i,j\rangle} \frac{J_{i,j}}{2}\left(b_i^\dagger b_j + b_j^\dagger b_i\right) + \frac{1}{2}\sum_j J_{i,j}^z n_j + \sum_j h_j\left(n_j - \frac{1}{2}\right). \quad (3.11)$$

We assume for simplicity $J_{i,j}^z$ to be site independent in the cluster, $J_{i,j}^z = J^z$. This is a Hamiltonian of independent particles and the reasoning of the previous section can be followed leading to a Hamiltonian for the cluster

$$H_c = -\sum_{\langle i,j\rangle} \left(t_{ij}|i\rangle\langle j| + \text{H.c.}\right) + \sum_j \left(\epsilon_j + \epsilon^z Z_j\right)|j\rangle\langle j| - \frac{1}{2}\left(\sum_j \epsilon_j\right)\hat{\mathbb{I}}, \quad (3.12)$$

with $J^z/2 = \epsilon^z$. One must not forget that at the contact sites, there is a extra neighbour which was not taken into account in the Hamiltonian. In order to correct this, an additional term must be added to the Hamiltonian of the cluster:

$$V_{LR}^z = -\epsilon_L^z |0\rangle\langle 0| - \epsilon_R^z |N_c\rangle\langle N_c|, \quad (3.13)$$

where $\epsilon_L^z = \frac{J_L^z}{2}$, $\epsilon_R^z = \frac{J_R^z}{2}$ and $|0\rangle$ and $|N\rangle$ represent the contact sites. Since we will consider a weak coupling between the leads and the cluster, it can be neglected. The fact that ϵ^z is different from zero introduces an additional term $\epsilon^z Z_j$ to the on-site energy. One can consider that $\epsilon_j + \epsilon^z Z_j$ is a new on-site energy which depends on the coordination number. This dependency can be seen as the introduction of local potentials whose intensity depend linearly with Z_i. This effect is discussed further in section 3.6.

Table 3.1: Correspondence between variables used in the hard-core Hamiltonian and the variables used in the tight-binding Hamiltonian.

Heisenberg Hamiltonian variables	Hard-core tight-binding Hamiltonian variables
$J/2$	t
h	ϵ
$J^z/2$	ϵ^z

3.4 Quantum scattering and transmittance.

In this section, the transmittance expression of a single magnon through a ferromagnetic cluster connected to two semi-infinite (modelled as ferromagnetic chains) leads is obtained. The followed approach only requires the understanding of the tight-binding model. The use

of Green's functions (for example as in electron conductance calculations such as the Meir-Wingreen formulation which is based on the non-equilibrium Green's functions method and takes into account electronic interactions in the cluster) [27, 28] or the traditional quantum scattering approach (which is a one-particle description of scattering events due to potential barriers) are avoided. [18] This approach is further simplified by the fact that the particles are confined to 1D ferromagnetic leads, and consequently no angle dependence is present in the transmittance expressions.[18] In nanoscale devices, the wavelike nature of the magnon must be taken into account and the quantum scattering description of the transmittance of a 1D particle across a structural or potential barrier is closely analogous to the Fresnel description of a plane light wave incident in a interface between two dielectric media. The wavefunction of a particle with momentum k and energy ε_k is written as an incident wave plus reflected and transmitted waves with amplitudes $r(\varepsilon_k)$ and $t(\varepsilon_k)$ respectively, relatively to the incident wave. The transmittance probability for this incident wave is $\mathcal{T} = |t(\varepsilon_k)|^2$. The hoppings $t_L = \frac{J_L}{2}$ and $t_R = \frac{J_R}{2}$ generate finite transmittance probability of the magnon across the cluster. Since no two-particles interactions are considered in this chapter, the transmittance probability for an incident magnon with momentum k and energy $\varepsilon_k = -2\cos(k)$ [recall that the energy of a magnon in a 1D ferromagnet is $\varepsilon_k = J^z - J\cos(k)$; so we set the zero energy at J^z, so that $\varepsilon_k \to -J\cos(k)$] can be calculated solving directly the respectively eigenvector equation for the tight-binding Hamiltonian. The method is very similar to that followed in the determination of the band structure of a tight-binding model. If we denote the eigenfunction amplitudes at sites n by ψ_n, the eigenvector equation $H(\psi) = \varepsilon_k(\psi)$ generates a system of N_t equations of the form

$$\varepsilon_k \psi_n = \sum_m^{N_t} H_{nm}\psi_m, \tag{3.14}$$

where $H_{nm} = \langle n|\hat{H}|m\rangle$ and N_t is the total number of sites in our system (it will be infinite since the leads are semi-infinite). The matrix element H_{nm} is zero except if the site m is a nearest-neighbor of site n or if $n = m$. One should now recall that our system is constituted by the left lead, the cluster and the right lead. If $t_L = t_R = 0$, the system of equations decouples into three independent sets of equations and the particle can be restricted to one of the three regions.

Let us now assume finite t_L and t_R. Since we are interested in the transmittance probability of a right-moving boson, we can limit our study to states with energy $\varepsilon_k = -2\cos(k)$ which can be written as an incident wave plus the respective reflected wave on the left lead and a transmitted wave on the right lead. This implies that the equations for the wavefunction amplitude at any site j of the leads (with $j < 0$ or $j > N_c + 1$),

$$\varepsilon_k \psi_j = -\psi_{j+1} - \psi_{j-1}, \tag{3.15}$$

are automatically satisfied if the wavefunction in the leads is of the form

$$\psi_j = e^{ikj} + \psi_r e^{-ikj}, \quad j \leq 0, \tag{3.16}$$

$$\psi_j = \psi_t e^{ikj}, \qquad j \geq N_c + 1, \tag{3.17}$$

where ψ_r and ψ_t are the amplitudes of the reflected and transmitted waves, respectively. These equations can be dropped from the the global system of equations. The equations describing the leads' behaviour are general and do not depend on the cluster structure. This is not

the case, however, for the cluster and the coupling leads-cluster. The following equations are developed for the particular case when the cluster is an open ring. The eigenvectors and eigenvalues when the boson is confined to the cluster are obtained from $H_c(\psi_c) = \epsilon(\psi_c)$ and the corresponding equations are of the form

$$\varepsilon_k \psi_j = \epsilon_j \psi_j - t\psi_{j+1} - t\psi_{j-1} \tag{3.18}$$

with periodic boundary conditions, $\psi_{N_c+1} = \psi_1$, where N_c is the number of sites in the cluster.

It remains the equations for the amplitudes at sites 0 and N_c+1 which involve the hopping constants t_L and t_R and depend on the amplitudes ψ_L and ψ_R at the sites L and R of the ring,

$$\varepsilon_k \psi_0 = -t_L \psi_L - \psi_{-1}, \tag{3.19}$$

$$\varepsilon_k \psi_{N_c+1} = -\psi_{N_c+2} - t_R \psi_R. \tag{3.20}$$

The amplitude equations at ring sites remain the same when t_L and t_R are finite, that is, $H_S(\psi_S) = \varepsilon_k(\psi_S)$, except for the equations corresponding to sites L and R which have an additional term $-t_L\psi_0$ and $-t_R\psi_{N_c+1}$ and are given by

$$\varepsilon_k \psi_L = -t_L \psi_0 + \epsilon_L \psi_L - t\psi_{L+1} - t\psi_{L-1}, \tag{3.21}$$

$$\varepsilon_k \psi_R = -t_R \psi_{N_c+1} + \epsilon_R \psi_R - t\psi_{R+1} - t\psi_{R-1}. \tag{3.22}$$

The solution of this set of $N_c + 2$ equations (that is, Eqs. 3.18, 3.19, 3.20, 3.21, and 3.22) allows to determine ψ_t and ψ_r. Note that ψ_0, ψ_{-1}, ψ_{N_c+1} and ψ_{N_c+2} are given by Eqs. 3.16 and 3.17 and therefore are functions of ψ_r and ψ_t. The transmittance probability is then given by the square of the absolute value of the ratio between the amplitude of the outgoing wave ψ_t and the amplitude of the incident wave (which is assumed to be 1).

3.5 Results

The previous discussion is used to determinate the transmittance of a non-interacting particle through tight-binding rings. We begin by presenting the influence of the structure of the cluster on the transmittance without an local external magnetic field. One of the simplest cases is a symmetric ring with site independent $\epsilon^z_{i,j} = \epsilon^z$, $t_{i,j} = t$ and $\epsilon_j = \epsilon$. A site independent ϵ_j allows to express $\sum_j \epsilon_j |j\rangle\langle j| - \frac{1}{2}\left(\sum_j \epsilon_j\right)\hat{\mathbb{I}}$ as $\sum_j \epsilon\left(1 - \frac{N_c}{2}\right)\hat{\mathbb{I}}$. In the particular case of symmetric ring, the number of neighbours Z_i is constant and equal to two. A site independent ϵ^z traduces in a constant diagonal term. Changing ϵ or ϵ^z produces equal shifts to all energy levels. These shifts, however, do not change the eigenstates of the system. The values of ϵ and ϵ^z should be calibrated such that the difference between eigenvalues remains within the leads' magnons allowed energies, otherwise the magnons cannot be transmitted by any of the cluster's states and no transmittance is allowed.

Upon the arrival of a magnon to the cluster, the associated plane wave gets splitted between the two arms of the ring. The waves travelling in the two arms will interfere and create a standing wave. This wave can either be one of the eigenstates of the decoupled ring, as seen in table 3.2, or a linear combination of the latter.

Table 3.2: The eigenstates of a symmetric ring with 8 sites, with $\epsilon^z = 0$, $\epsilon^z_{\text{Leads}} = 0$, $\epsilon^z_L = \epsilon^z_R = 0$ and $\epsilon = 0$. The grey areas represent the probability density of the eigenstates with the respective momentum.

Energy Spectra	Momentum (rad/site)	Wavelength (Sites)	Probability Density, $\lvert\psi(\epsilon)\rvert^2$	Probability Density, $\lvert\psi(\epsilon)\rvert^2$ (For degenerate states)
$-2t\cos(\pi)$	$\frac{2\pi}{2}$	2	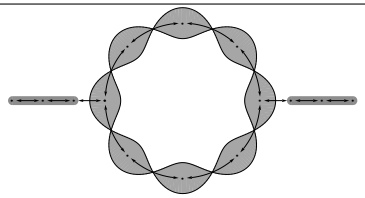	
$-2t\cos\left(\pi - \frac{\pi}{4}\right)$	$\frac{3*2\pi}{8}$	$\frac{8}{3}$	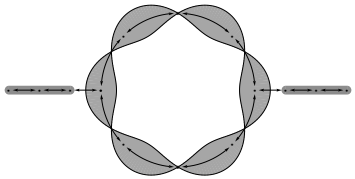	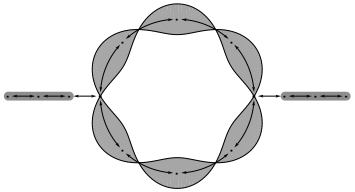
0	$\frac{2\pi}{4}$	4	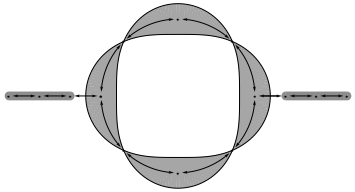	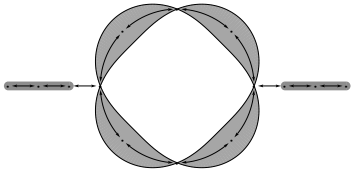
$-2t\cos(\frac{\pi}{4})$	$\frac{2\pi}{8}$	8	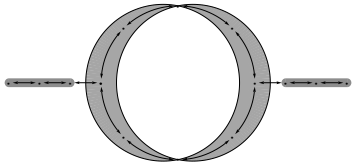	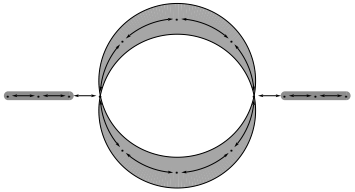
$-2t$	0	∞	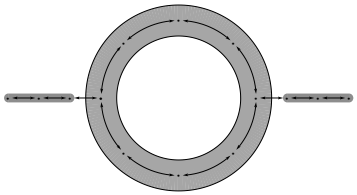	

The plotted probability densities shown in table 3.2 are continuous to highlight the effects produced by the different frequencies. The transmittance profiles will show peaks when the energy of the incident particle/magnon coincides with an energy level of the cluster (in chapter 4 we show that for $N_\uparrow \neq 0$, the energy of the incoming magnon must match the energy difference between the ground state with $N_\uparrow$ and any of the states with $N_\uparrow \pm 1$; the only state with $N_\uparrow = 0$ is the empty state whose energy is zero). Some of these peaks are absent and this can be related to the probability density of the eigenstates of the cluster Hamiltonian, as discussed below. States with different momentums may have the same probability profile. Taking, for instance, the states with momentum $\frac{2\pi}{2}$ and 0, one can see that, although the wavefunctions have equal or symmetric values on the sites, the probability is equal for both cases. The same can be said for each of the wavefunctions with momentum $\frac{3*2\pi}{8}$ and $\frac{2\pi}{8}$, as seen in fig. 3.2.

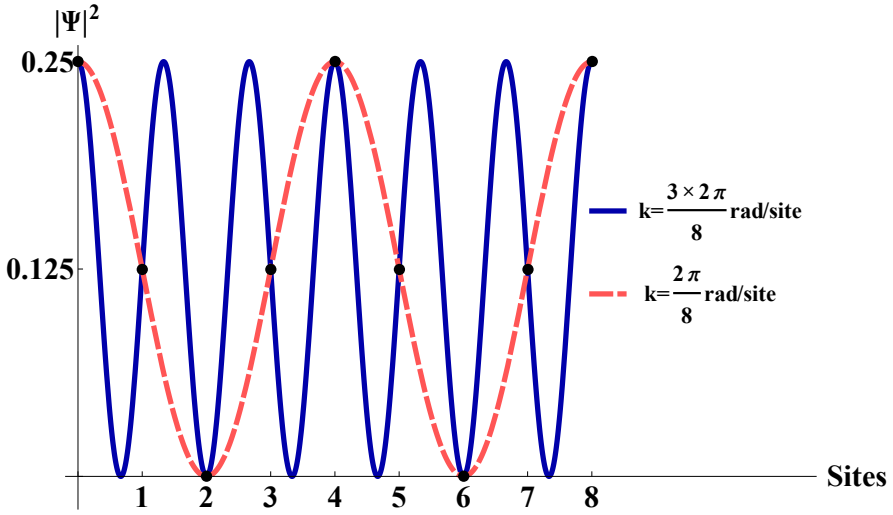

Figure 3.2: Plot of the probability density for standing waves with momentum $k = \frac{3*2\pi}{8}$ and $k = \frac{2\pi}{8}$. Although the probability densities are different, their values at each site are equal.

The transmittance of magnons ultimately depends on the probability density at the contact sites and the difference of energy between the incoming magnon and the eigenstates of the cluster. The eigenstates can be classified as transmitting and non-transmitting depending on the value of the probability density at the contacts. An eigenstate is said to be non-transmitting if the probability of the presence of a magnon at either contact sites is zero. Otherwise, the eigenstate is said to be transmitting. In the particular case of a 8 site ring, the probability density on the contacts is either a maximum or a minimum equal to zero. This means that, apart from the energy dependence that is developed further next, each eigenstate either allows perfect transmittance, $\mathcal{T} = 1$, or no transmittance at all, $\mathcal{T} = 0$. A magnon is not transmitted along the cluster if the energy is not close enough. Small t_L and t_R produce sharp pikes of transmittance for magnons energies around the transmitting eigenstates energies. Large t_L and t_R allows a wider range of magnon energies to be transmitted. A cluster state can only transmit magnons with almost equal energy and if it is a transmitting state. If neither of the two conditions is met, the magnon is not transmitted.

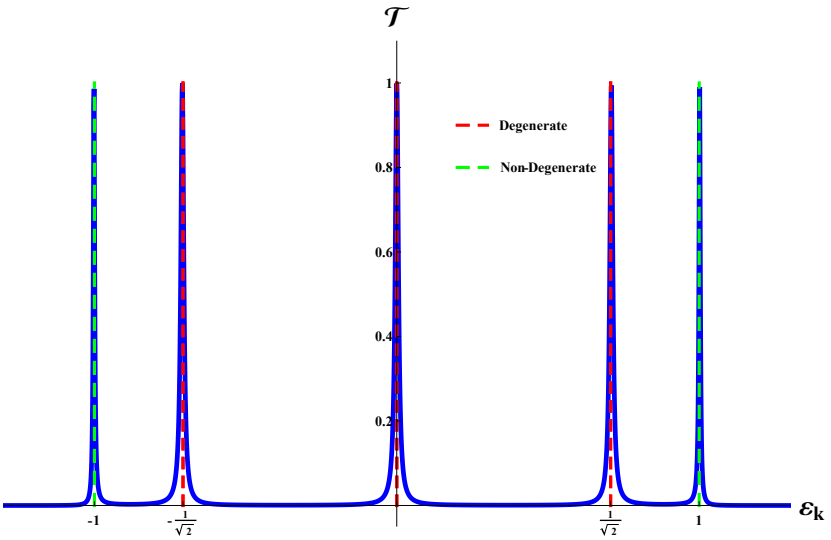

Figure 3.3: Transmittance of magnons with ε_k through a perfect 8 sites ring with $\epsilon = 0$, $t = 0.5$, $t_L = t_R = 0.1125$, $\epsilon^z = 0$ and $\epsilon^z_L = \epsilon^z_R = 0$. The red and green dashed lines indicate degenerate and non-degenerate eigenenergies of the cluster, respectively.

3.6 Iron Clusters and Local Potentials

As seen previously, ϵ^z introduces local potentials whose intensities depends on the coordination number of each site. A variety of structures present variable Z_i. A family of structures that present non-homogeneous Z_i is the Fe_n clusters. These clusters have been studied in order to understand the phenomena of orbital quenching in non-crystalline mesoscopic structures. [29] Although the atoms of these structures present a variety of total magnetic moments, [30, 31] for simplicity the magnetic moment of each site will considered to be equal to an electron magnetic moment μ_B. One simple iron cluster is the Fe_7 structure with seven sites as seen in fig. 3.4. The sites in the pentagon plane have four neighbours while the other two sites have five. This produces an energetic distinction between the pentagon sites and the central sites. Changes in the value of ϵ^z lead to shifts which depend on the wavefunction's amplitudes. The overall width of the peaks depend on the values of t_L and t_R, but the individual transmittance peaks' widths and heights depend on the amplitudes of the wavefunction on the contacts. This allows to distinguish between the degenerate states. Although equal in energy, the amplitudes on the contacts for the degenerate states are distinct. In fig. 3.4, the distinction between degenerate states is possible as the peaks have distinct widths and heights. The transmittance peaks with close energies have complex behaviours due to the interference of the respective wavefunctions. Two transmitting states, i.e. states with amplitude bigger than zero at the contacts, with close energies will interfere constructively or destructively depending on the phases on the contacts. If a completely destructive interference occurs (at the contacts) the transmittance falls to zero. This can be seen in fig. 3.4 where each degenerate state produces a peak in transmittance which abruptly falls to zero for the energy of degenerate states. The local potentials on this cluster becomes evident when changing ϵ^z as presented in table 3.3. The local potential energy shift varies according to the eigenstate and it is ruled by $\epsilon^z \sum_j Z_j |j\rangle\langle j|$. Whenever an eigenstate only has finite amplitude at sites with same number

of neighbours, this expression can be written as $\epsilon^z Z_j \sum_j |j\rangle\langle j| \equiv \epsilon^z Z_j \hat{\mathbb{I}}$. The degenerate states in table 3.3 only have finite amplitude at sites with $Z_i = 4$. The energy shift in table 3.3 is given by $\Delta E_c = E_c\left(\epsilon^z = \frac{1}{8}\right) - E_c\left(\epsilon^z = -\frac{1}{8}\right) = E_c(\epsilon^z = 0) + \frac{4}{8} - \left(E_c(\epsilon^z = 0) - \frac{4}{8}\right) = \frac{2\times4}{8} = 1$. The same reasoning can be followed in the case of the state with $\left(\epsilon^z = \frac{1}{8}\right) = 0.6250$ but with $Z_i = 5$: $\Delta E_c = \frac{2\times5}{8} = 1.2500$. The other states present values of ΔE_c between 1 and 1.2500.

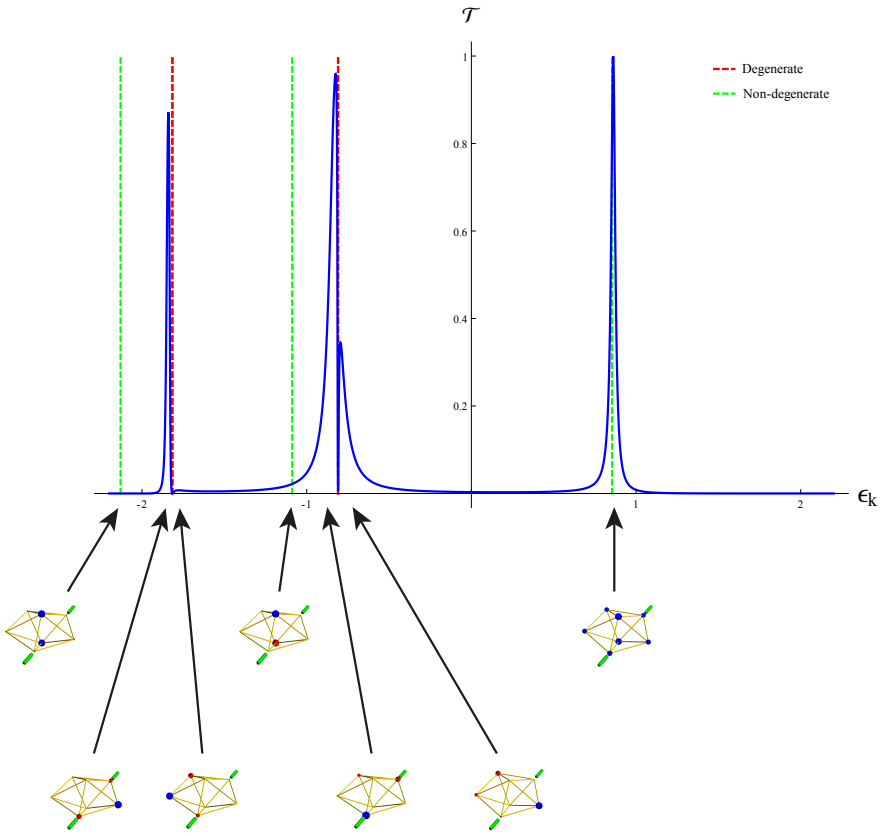

Figure 3.4: Transmittance of magnons with energy ε_k through a Fe_7 cluster with $\epsilon = 0$, $t = 0.5$, $t_L = t_R = 0.1125$, $\epsilon^z = 0$, $\epsilon^z_{\text{Leads}}$ and $\epsilon^z_L = \epsilon^z_R = 0$. The vertical lines represent the energies of the cluster's wavefunctions which are indicated below. The green thick lines in the diagrams represent the leads connecting with the cluster. The yellow lines represent the possible hoppings between sites. The amplitude and phase of the wavefunction on each site is represented by the radius and colour of the sphere at that site, respectively. The phase can have values between 0 and π which are represented by a colour gradient from blue to red.

3.7 Magnetic Tip

Previously, the external magnetic field was considered to be uniform or null. The influence of a non-uniform local magnetic field in the transmittance through clusters is now discussed.

Table 3.3: Energy shift produced by the local potential due to non-homogeneous Z_i in a Fe_7 cluster with $\epsilon = 0$, $t = 0.5$, $t_L = t_R = 0.2$ and $\epsilon_L^z = \epsilon_R^z = 0$ and for $\epsilon^z = \frac{1}{8}$ and $\epsilon^z = -\frac{1}{8}$. The four degenerate states have zero density probability at the central sites. This means that the wavefunctions only have finite amplitude at sites with four neighbours. On the contrary, the state with $E_c\left(\epsilon^z = \frac{1}{8}\right) = 0.0625$ has zero density probability at the pentagon's sites. The other states have components at every site.

States		$E_c\left(\epsilon^z = \frac{1}{8}\right)$	$E_c(\epsilon^z = -\frac{1}{8})$	ΔE_c
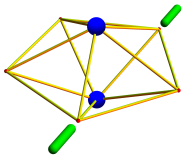		-0.5780	-1.7407	1.1627
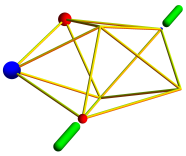	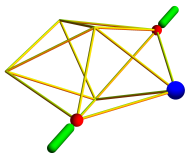	-0.3090	-1.3090	1.0000
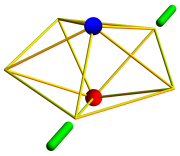		0.6250	-0.6250	1.2500
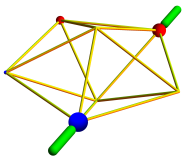	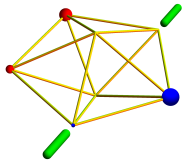	0.8090	-0.1910	1.0000
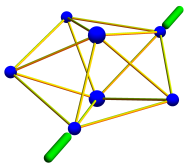		2.70305	1.6157	1.0873

A radial magnetic field may be generated by a magnetic tip in the proximity of the ring. The intensity of the magnetic field decreases with the distance to the centre of the tip and we assume it is given by a Gaussian function $H(\vec{r},\vec{t}) = H_0 e^{-\frac{(\vec{r}-\vec{t})^2}{2c^2}}$, where $\vec{r}$ is the magnetic field intensity measurement position, $\vec{t}$ is the position of the tip, H_0 is the magnetic field intensity at the tip and c is the Gaussian function standard deviation. Other forms of local magnetic fields should lead to similar results. The possibility of particle hoppings between the cluster and the magnetic tip is neglected, as well as the effect of the magnetic field in the leads. As in the case of the uniform magnetic field, this field changes the on-site energy, which is now given by $\epsilon_j n_j \rightarrow \epsilon_j n_j + H(\vec{r_j},\vec{t})\left(n_j - \frac{1}{2}\right)$, where $\vec{r_j}$ is the position of the site j. The tip is kept at a fixed distance z of the ring plane and its position is swept in the x and y directions while the transmittance being calculated for each tip position. The respective contour plots are shown in fig. 3.5a, 3.5b, 3.5c, 3.5d, 3.5e, 3.5f, 3.5g, 3.5h and 3.5i. In general, we observe in these contour plots, peaks or dips in the transmittance when the tip (x, y) position comes close to a site of the ring. This, however is not always verified for all sites. A fine tuned set of conditions enables to relate the absence of some of this peaks with the energy levels of the cluster. Consider the perfect 8 sites ring with $t = 0.125$, $\epsilon^z = 0$, $\epsilon^z_{\text{Leads}} = 0$, $\epsilon^z_L = \epsilon^z_R = 0$ and $\epsilon = 0$. In this case the energy levels for the decoupled ring are $E_c(N_\uparrow = 1) = \{-0.25t, -0.25\cos\left(\frac{\pi}{4}\right), 0, -0.25\cos\left(\pi - \frac{\pi}{4}\right), -0.25\cos(\pi)\} \approx \{-0.2500, -0.1768, 0.0000, 0.1768, 0.2500\}$. Sending spin waves with energy slightly shifted from one of the eigenenergies produces a transmittance much smaller than 1 because the transmittance peaks are sharp around the eigenenergies (for small values of t_L and t_R). If a tuned magnetic tip (i.e. with ideal H_0, c and z) sweeps the surface, the shift of energy produced by the tip can compensate the spin wave energy shift and produce total transmittance. This effect was used in figures 3.5d, 3.5e,3.5f, 3.5g and 3.5h to obtain an image of the probability density profiles of the eigenstates of the ring. When using this effect one may expect the magnetic tip transmittance shift to be site independent (i.e. putting the tip above each site produces the same transmittance). If this was the case, the contour plot for every eigenstates would have peaks in every site, as seen in figures 3.5d and 3.5h. The magnetic tip transmittance shift, however, is not site independent but it depends on the amplitude of the eigenfunction with energy close to that of the incoming spin wave. As seen previously on section 3.5, an incoming magnon can only be transmitted by states with energy close to its own. For sufficiently spaced energy spectrum of the cluster, only one state (if non-degenerations are present) will contribute for the transmittance. This means that for the magnon to be transmitted the tip must be close to a site where the amplitude of eigenstate in question is not-null thus creating a spatial profile of the amplitude of the eigenstate. This can be verified by comparing figures 3.5d, 3.5e, 3.5f, 3.5g and 3.5h with the ones present in table 3.2. When considering degenerate states, it is expected that each state contribute to the transmittance. For a transmittance contour plot, the degenerate states should appear as a overlap of each probability densities. This is not verified in the case of the perfect ring because for each degeneracy only one of the two states is transmitting. Even though the magnetic tip can compensate the energy shifts, these states never appear in the transmittance plot. It is not expected to observe transmittance for states with zero density probability at the contacts.

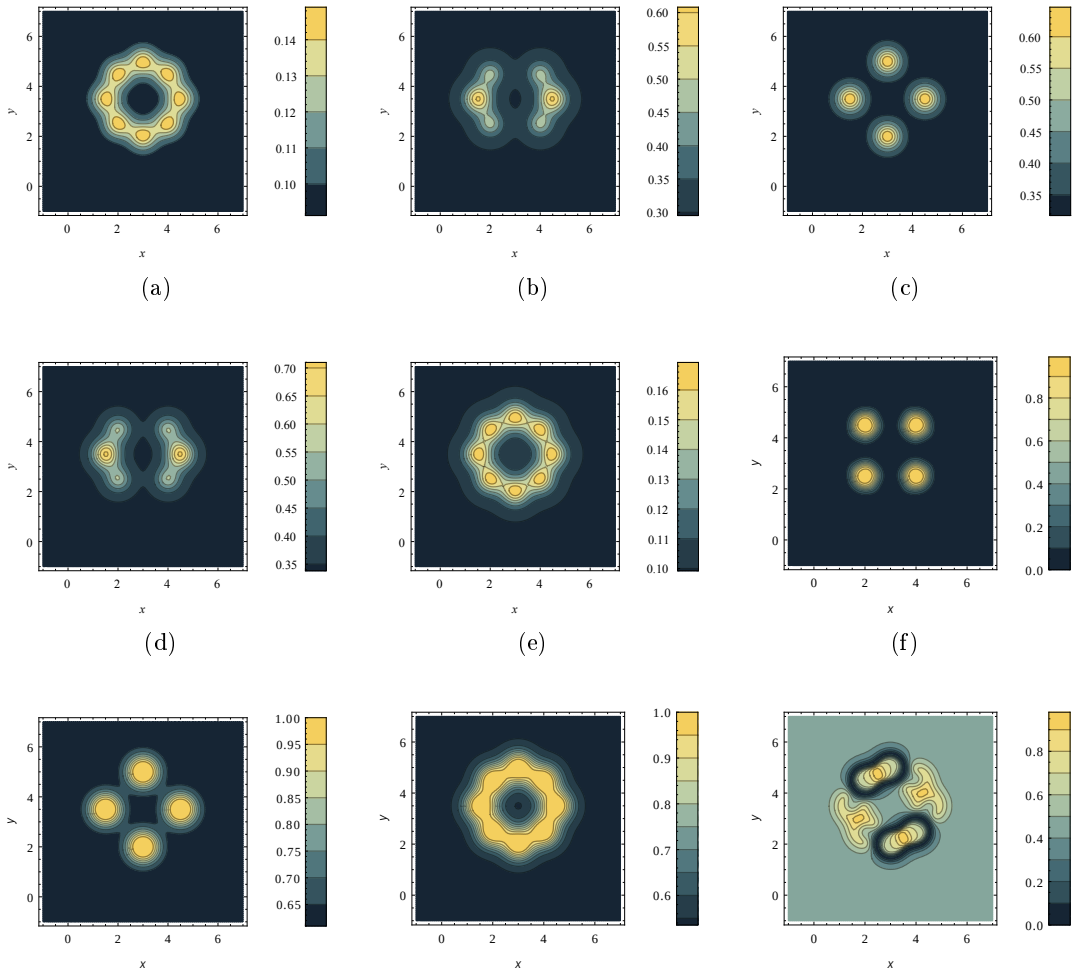

Figure 3.5: Transmittance contour plots of a ring with 8 sites. The contacts in plots (a), (b), (c), (d) and (e) are placed at opposite sites of the ring. The contacts in plots (f) and (g) are placed at sites of the ring forming a 90^{o} angle in between. The contacts in plots (h) and (i) are placed at sites of the ring forming a 135^{o} angle in between. The contour plots are a function of the position $\vec{t} = (x, y, z)$ of the magnetic tip for several conditions. The commom variable used in all plots are $\epsilon = 0$, $\epsilon^{z} = 0$, $\epsilon^{z}_{Leads} = 0$,$\epsilon^{z}_{L} = \epsilon^{z}_{R} = 0$, $t = 0.125$, $t_L = t_R = 0.09999$, $H_0 = 4$, $c = 0.425$, $z = 1.9$. The energies of the incoming magnons are the following: (a) $\varepsilon_k = -0.2500 + 0.0001$, (b) $\varepsilon_k = -0.1768 + 0.0001$, (c) $\varepsilon_k = 0.0000 + 0.0001$, (d) $\varepsilon_k = 0.1768 + 0.0001$, (e) $\varepsilon_k = 0.2500 + 0.0001$, (f) $\varepsilon_k = -0.17678 + 0.00002$, (g) $\varepsilon_k = 0.00000 + 0.00004$, (h) $\varepsilon_k = -0.25000 + 0.00002$ and (i) $\varepsilon_k = -0.17678 + 0.00002$. The first value of each energy is the eigenvalue while the second term is the shift used to produce the images.

Chapter 4

Generalization for clusters with arbitrary magnetization

In the previous chapter, the transmittance of magnons through a fully ferromagnetic system was discussed. A more general system can be described if interactions between magnons are considered. The leads are still considered to be perfectly ferromagnetic. The cluster can, however, have any magnetic phase. The magnetization associated with the magnetic phase is a measurement of the number of magnons present in the cluster and it is given by $M(N_\uparrow) = -N_c/2 + N_\uparrow$, being $N_\uparrow \in \{0, 1, 2, ..., N_c\}$ the number of magnons present in the cluster. The regular tight-binding approach used previously to calculate the transmittance requires modifications in order to deal with multiple magnons, since the interacting terms have to added to the tight-binding Hamiltonian. To simplify this problem a tunnelling perspective was adopted, that is, we consider an incoming magnon from the left lead and we assume that this magnon will be partially transmitted through the cluster to the right lead. This implies that the number of magnons in the cluster remains fixed except when the incoming magnon arrives at the cluster. [32] We begin by describing the restrictions necessary to compute the transmittance of the magnon which we will apply in the case of an Fe_{13}^{+} cluster.

4.1 Restricted subspace for magnon transmittance

The magnon must tunnel from a lead to one of the cluster contacts and then tunnel from the other contact to the other lead in order to be transmitted. It is recommended to separate the system space into three sub-spaces in order to better express the following approximations and calculations. The system space is represented by a set of three kets: the first ket belongs to the left lead subspace, the second to the cluster subspace and the third to the right lead subspace. In order for this approach to be implemented two approximations were required:

- There can be at most one particle in each lead. This implies that interaction between magnons is not considered in the leads.

- As a consequence of the previous approximation, the allowed subspace of states is:

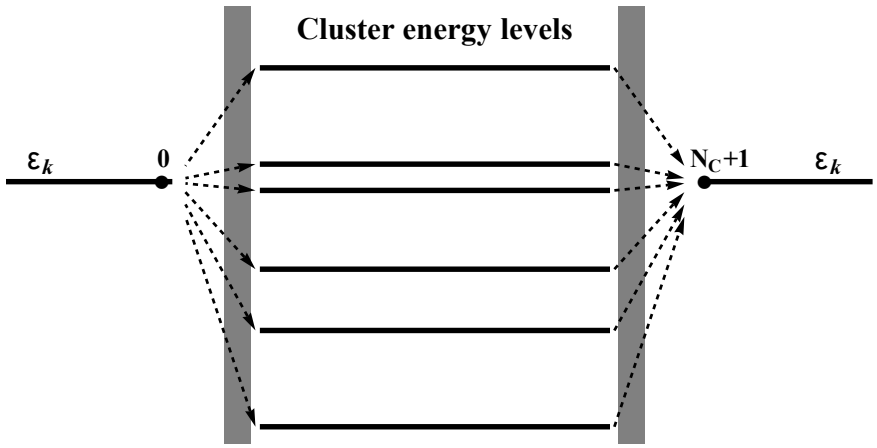

Figure 4.1: Schematic representation of the tunnelling approach. The left and right lines represent the incoming magnon energy. The central lines represent energy levels of the cluster that are described in the body of the text.

$$\text{"Incoming"} \quad b_i^\dagger \left|\emptyset_L\right\rangle \otimes \left|\mathrm{GS}(N_\uparrow)\right\rangle \otimes \left|\emptyset_R\right\rangle, \quad i<0, \tag{4.1}$$

$$\text{"Transmitted"} \quad \left|\emptyset_L\right\rangle \otimes \left|\mathrm{GS}(N_\uparrow)\right\rangle \otimes b_j^\dagger \left|\emptyset_R\right\rangle, \quad j>N_c+1, \tag{4.2}$$

$$\text{"Cluster}\,(N_\uparrow+1)\text{"} \quad \left|\emptyset_L\right\rangle \otimes \left|N_\uparrow+1_{(n)}\right\rangle \otimes \left|\emptyset_R\right\rangle, \tag{4.3}$$

$$\text{"Cluster}\,(N_\uparrow-1)\text{"} \quad b_0^\dagger \left|\emptyset_L\right\rangle \otimes \left|N_\uparrow-1_{(m)}\right\rangle \otimes b_{N_c+1}^\dagger \left|\emptyset_R\right\rangle, \tag{4.4}$$

where $b_j^\dagger$ is the hard-core boson creation operator described in section 2.1, $\left|\emptyset_L\right\rangle$ and $\left|\emptyset_R\right\rangle$ are the fully ferromagnetic left and right leads states, respectively, and $\left|\mathrm{GS}(N_\uparrow)\right\rangle$ is the ground state of the cluster with $N_\uparrow$ magnons, $\left|N_\uparrow+1_{(n)}\right\rangle$ represents the n^{th} state out of $\binom{N_c}{N_\uparrow+1}$ eigenvectors with $N_\uparrow+1$ magnons and $\left|N_\uparrow-1_{(m)}\right\rangle$ represents the m^{th} state out of $\binom{N_c}{N_\uparrow-1}$ eigenvectors with $N_\uparrow-1$ magnons. The ferromagnetic leads are described as empty states because full ferromagnetic states are characterized by the absence of flipped spins, i.e. magnons.

The goal is to calculate the transmittance for an incoming magnon which far from the cluster is in a plane wave state. Any incident wave packet can obviously be written as a linear combination of these eigenstates. For the left lead ($j \ll 0$) one has an incident and reflected wave

$$\left(e^{ikj}+\psi_r e^{-ikj}\right) b_j^\dagger \left|\emptyset_L\right\rangle \otimes \left|\mathrm{GS}(N_\uparrow)\right\rangle \otimes \left|\emptyset_R\right\rangle. \tag{4.5}$$

For the right lead ($j \gg N_c+1$) one has a transmitted wave

$$\psi_t e^{ikj} \left|\emptyset_L\right\rangle \otimes \left|\mathrm{GS}(N_\uparrow)\right\rangle \otimes b_j^\dagger \left|\emptyset_R\right\rangle. \tag{4.6}$$

The ground state of the cluster is assumed to be the same as that of the decoupled system, which is a valid approximation given that the hybridization between the leads and the cluster is assumed to be small. The rest of the eigenstates can be constructed from these far away components. Given the energy eigenstate $\left|\Psi_k\right\rangle$ of energy $E=\varepsilon_k+E_{\mathrm{GS}(N_\uparrow)}$, where ε_k is the

energy of the incident particle and $E_{\mathrm{GS}(N_\uparrow)}$ is the energy of the cluster with $N_\uparrow$ particles and the restriction to the subspace in 4.1, then for the "far away" components we have

$$H\left|\Psi_k\right\rangle \to \left(H_{\text{leads}} \sum_{j \text{ far}} \psi_j b_j^\dagger \left|\emptyset\right\rangle \otimes \left|\mathrm{GS}(N_\uparrow)\right\rangle + \sum_{j \text{ far}} \psi_j b_j^\dagger \left|\emptyset\right\rangle \otimes H_{\mathrm{c}} \left|\mathrm{GS}(N_\uparrow)\right\rangle \right). \tag{4.7}$$

Hence

$$H\left|\Psi_k\right\rangle = \left(\varepsilon_k + E_{\mathrm{GS}(N_\uparrow)}\right)\left|\Psi_k\right\rangle \tag{4.8}$$

leads to

$$H_{\text{leads}} \sum_{j \text{ far}} \psi_j b_j^\dagger \left|\emptyset\right\rangle = \varepsilon_k \sum_{j \text{ far}} \psi_j b_j^\dagger \left|\emptyset\right\rangle \tag{4.9}$$

as expected. If the non-interacting reasoning of the previous chapter is followed, then the incoming (and reflected) components of $\left|\Psi_k\right\rangle$ ($j \leq 0$)

$$\left(e^{ikj} + \psi_r e^{-ikj}\right) b_j^\dagger \left|\emptyset_L\right\rangle \otimes \left|\mathrm{GS}(N_\uparrow\right\rangle \otimes \left|\emptyset_R\right\rangle \tag{4.10}$$

and the transmitted components ($j \geq N_c + 1$) are

$$\psi_t e^{ikj} \left|\emptyset_L\right\rangle \otimes \left|\mathrm{GS}(N_\uparrow\right\rangle \otimes b_j^\dagger \left|\emptyset_R\right\rangle. \tag{4.11}$$

Theses states have the same expressions as those for the case when the magnon is far away from the cluster. The full form of the eigenstate with energy $\varepsilon_k + E_{\mathrm{GS}(N_\uparrow)}$ in the restricted subspace is

$$\begin{aligned} \left|\Psi_k\right\rangle = & \sum_{j \leq 0} \left(e^{ikj} + \psi_r e^{-ikj}\right) b_j^\dagger \left|\emptyset_L\right\rangle \otimes \left|\mathrm{GS}(N_\uparrow)\right\rangle \otimes \left|\emptyset_R\right\rangle \\ & + \sum_{j \geq N_c+1} \psi_t e^{ikj} \left|\emptyset_L\right\rangle \otimes \left|\mathrm{GS}(N_\uparrow)\right\rangle \otimes b_j^\dagger \left|\emptyset_R\right\rangle \\ & + \sum_n \left|\emptyset_L\right\rangle \otimes \alpha_n \left|N_\uparrow + 1_{(n)}\right\rangle \otimes \left|\emptyset_R\right\rangle \\ & + \sum_m b_0^\dagger \left|\emptyset_L\right\rangle \otimes \beta_m \left|N_\uparrow - 1_{(m)}\right\rangle \otimes b_{N_c+1}^\dagger \left|\emptyset_R\right\rangle \end{aligned} \tag{4.12}$$

The first and second summation sum over the left and right leads' positions for the incoming magnon, respectively. The third summation sums over all $\binom{N_c}{N_\uparrow + 1}$ eigenstates of the cluster with $N_\uparrow + 1$ magnons, where the last summation sums over all $\binom{N_c}{N_\uparrow - 1}$ eigenstates of the cluster with $N_\uparrow - 1$ magnons, α_n and β_m are the respective amplitudes. Our objective is to determine ψ_t. This is achieved noting that the components of $\left|\Psi_k\right\rangle$

$$\begin{aligned} & \psi_0 b_0^\dagger \left|\emptyset_L\right\rangle \otimes \left|\mathrm{GS}(N_\uparrow)\right\rangle \otimes \left|\mathrm{O}_R\right\rangle \\ & \psi_{N_c+1} \left|\emptyset_L\right\rangle \otimes \left|\mathrm{GS}(N_\uparrow)\right\rangle \otimes b_{N_c+1}^\dagger \left|\emptyset_R\right\rangle \\ & \sum_n \left|\emptyset_L\right\rangle \otimes \alpha_n \left|N_\uparrow + 1_{(n)}\right\rangle \otimes \left|\emptyset_R\right\rangle \\ & \sum_m b_0^\dagger \left|\emptyset_L\right\rangle \otimes \beta_m \left|N_\uparrow - 1_{(m)}\right\rangle \otimes b_{N_c+1}^\dagger \left|\emptyset_R\right\rangle. \end{aligned} \tag{4.13}$$

must obey to the eigenvalue equation, where

$$\psi_j = \begin{cases} e^{ikj} + \psi_r e^{-ikj}, & j < 0 \\ \psi_t e^{ikj}, & j > N_c \end{cases} \tag{4.14}$$

The Schrödinger equation can now be used to compute ψ_t. The application of the Schrödinger equation produces an extensive expression which can be separated into the distinct components of $|\Psi_k\rangle$. For each distinct component the Schrödinger equation generates an equation and the solution of the system of these equations allows to determine the transmittance of the magnon wave. The action of the Hamiltonian in $|\Psi_k\rangle$ also produces states that do not fall within the restrict subspace and are therefore discarded. The Schrödinger equation for the component $b_0^\dagger |\emptyset_L\rangle \otimes |\mathrm{GS}(N_\uparrow)\rangle \otimes |\emptyset_R\rangle$ is given by

$$\begin{aligned} \left(\varepsilon_k + E_{\mathrm{GS}(N_\uparrow)}\right) \psi_0 b_0^\dagger |\emptyset_L\rangle \otimes |\mathrm{GS}(N_\uparrow)\rangle \otimes |\emptyset_R\rangle = \\ - \psi_{-1} b_0^\dagger |\emptyset_L\rangle \otimes |\mathrm{GS}(N_\uparrow)\rangle \otimes |\emptyset_R\rangle \\ - t_L b_0^\dagger |\emptyset_L\rangle \otimes \sum_m \alpha_m b_L |N_\uparrow + 1_{(m)}\rangle \otimes |\emptyset_R\rangle \\ - t_R b_0^\dagger |\emptyset_L\rangle \otimes \sum_n \beta_n b_R |N_\uparrow - 1_{(n)}\rangle \otimes |\emptyset_R\rangle \\ + E_{\mathrm{GS}(N_\uparrow)} \psi_0 b_0^\dagger |\emptyset_L\rangle \otimes |\mathrm{GS}(N_\uparrow)\rangle \otimes |\emptyset_R\rangle . \end{aligned} \tag{4.15}$$

For simplicity, the $b_0^\dagger |\emptyset_L\rangle$ and $|\emptyset_R\rangle$ factors are ignored as they are always present and do not contribute to the discussion:

$$\begin{aligned} \left[\left(\varepsilon_k + \cancel{E_{\mathrm{GS}(N_\uparrow)}}\right) \psi_0 + \psi_{-1}\right] |\mathrm{GS}(N_\uparrow)\rangle = - t_L \sum_n \alpha_n b_L |N_\uparrow + 1_{(n)}\rangle \\ - t_R \sum_m \beta_m b_R^\dagger |N_\uparrow - 1_{(m)}\rangle \\ + \cancel{E_{\mathrm{GS}(N_\uparrow)} \psi_0 |\mathrm{GS}(N_\uparrow)\rangle}. \end{aligned} \tag{4.16}$$

We are working in a restricted subspace, where the only available state with $N_\uparrow$ particles in the cluster is the ground state, $|\mathrm{GS}(N_\uparrow)\rangle$, so that it is required to project all states with $N_\uparrow$ to $|\mathrm{GS}(N_\uparrow)\rangle$:

$$\begin{aligned} \left[\varepsilon_k \psi_0 + \psi_{-1}\right] |\mathrm{GS}(N_\uparrow)\rangle = - t_L \sum_n \alpha_n |\mathrm{GS}(N_\uparrow)\rangle \langle \mathrm{GS}(N_\uparrow)| b_L |N_\uparrow + 1_{(n)}\rangle \\ - t_R \sum_m \beta_m |\mathrm{GS}(N_\uparrow)\rangle \langle \mathrm{GS}(N_\uparrow)| b_R^\dagger |N_\uparrow - 1_{(m)}\rangle , \end{aligned} \tag{4.17}$$

so that one obtains

$$\begin{aligned} \left[\varepsilon_k \psi_0 + \psi_{-1}\right] = - t_L \sum_n \alpha_n \langle \mathrm{GS}(N_\uparrow)| b_L |N_\uparrow + 1_{(n)}\rangle \\ - t_R \sum_m \beta_m \langle \mathrm{GS}(N_\uparrow)| b_R^\dagger |N_\uparrow - 1_{(m)}\rangle . \end{aligned} \tag{4.18}$$

The following parameters are introduced in order to simplify the notation:

$$t^L_{\alpha_n}(N_\uparrow) = t_L \langle N_\uparrow + 1_{(n)}| \, b_L^\dagger \, |\mathrm{GS}(N_\uparrow)\rangle \tag{4.19}$$

$$t^R_{\alpha_n}(N_\uparrow) = t_R \langle \mathrm{GS}(N_\uparrow)| \, b_R \, |N_\uparrow + 1_{(n)}\rangle \tag{4.20}$$

$$t^R_{\beta_m}(N_\uparrow) = t_R \langle N_\uparrow - 1_{(m)}| \, b_R \, |\mathrm{GS}(N_\uparrow)\rangle \tag{4.21}$$

$$t^L_{\beta_m}(N_\uparrow) = t_L \langle \mathrm{GS}(N_\uparrow)| \, b_L^\dagger \, |N_\uparrow - 1_{(m)}\rangle \tag{4.22}$$

$$\epsilon_{\alpha_n}(N_\uparrow) = E_{\alpha_n}(N_\uparrow - 1) - E_{GS}(N_\uparrow) \tag{4.23}$$

$$\epsilon_{\beta_m}(N_\uparrow) = E_{\beta_m}(N_\uparrow + 1) - E_{GS}(N_\uparrow). \tag{4.24}$$

Equation 4.18 becomes

$$\varepsilon_k \psi_0 + \psi_{-1} = -\sum_n \left(t^L_{\alpha_n(N_\uparrow)}\right)^* \alpha_n - \sum_m \left(t^R_{\beta_m(N_\uparrow)}\right)^* \beta_m. \tag{4.25}$$

Equation 4.25 is one of the equations that forms the wanted system of equations. The procedure must now be repeated for the remaining components of $|\psi_k\rangle$ to obtain the complete system. For $|\emptyset_L\rangle \otimes \alpha_n \, |N_\uparrow + 1_{(m)}\rangle \otimes |\emptyset_R\rangle$ one obtains

$$(\varepsilon_k - \epsilon_{\alpha_n}) \, \alpha_n = -\left(t^L_{\alpha_n(N_\uparrow)}\right) \psi_0 - \left(t^R_{\alpha_n(N_\uparrow)}\right)^* \psi_{N_c+1}. \tag{4.26}$$

For $b_0^\dagger \, |\emptyset_L\rangle \otimes \beta_n \, |N_\uparrow - 1_{(n)}\rangle \otimes b^\dagger_{N_c+1} \, |\emptyset_R\rangle$

$$(\varepsilon_k - \epsilon_{\beta_m}) \, \beta_m = -\left(t^L_{\beta_m(N_\uparrow)}\right)^* \psi_{N_c+1} - \left(t^R_{\beta_m(N_\uparrow)}\right) \psi_0. \tag{4.27}$$

Lastly, $|\emptyset_L\rangle \otimes |\mathrm{GS}(N_\uparrow)\rangle \otimes b^\dagger_{N_c+1} \, |\emptyset_R\rangle$ produces the last equation

$$\varepsilon_k \psi_{N_c+1} + \psi_{N_c+2} = -\sum_n \left(t^R_{\alpha_n(N_\uparrow)}\right) \alpha_n - \sum_m \left(t^L_{\beta_m(N_\uparrow)}\right) \beta_m. \tag{4.28}$$

This way one obtains a set of $2 + N_\alpha + N_\beta$ equations given by the expressions 4.25, 4.26, 4.27 and 4.28, where $N_\alpha = \binom{N_c}{N_\uparrow - 1}$ and $N_\beta = \binom{N_c}{N_\uparrow + 1}$. These equations allow to calculate the values of $2 + N_\alpha + N_\beta$ variables which are ψ_r, ψ_t, $\{\alpha_n\}$ and $\{\beta_m\}$. The values of ψ_r and ψ_t are obtained from the values of ψ_0, ψ_{-1},ψ_{N_c+1} and ψ_{N_c+2}. As in the tight-binding approach the transmittance probability is given by $\mathcal{T} = |\psi_t|^2$. The energy difference between states with $N_\uparrow + 1$ and the ground state with $N_\uparrow$, $\epsilon_{\alpha_n}(N_\uparrow)$, and the energy difference between states with $N_\uparrow - 1$ and the ground state with $N_\uparrow$, $\epsilon_{\beta_m}(N_\uparrow)$, define which incoming magnons have the right energy to be transmitted. As in the previous approach, the energy of the incoming magnon must match either $\epsilon_{\alpha_n}(N_\uparrow)$ or $\epsilon_{\beta_m}(N_\uparrow)$ in order to be transmitted. This tunnelling approach can be compared with the tight-binding approach of the previous approach when considering the absence of magnons on the cluster. Special care is required when considering $N_\uparrow = 0$. Firstly, one must note that the states $|N_\uparrow - 1_{(n)}\rangle$ are not defined. States with -1 particles do not have physical meaning, therefore they were not used in the computations. Secondly, there is only one state with 0 particles, $|\emptyset_c\rangle = |000...\rangle$. As such it is the ground-state whose energy

is $\epsilon_{\mathrm{GS}}(0) = 0$. With these considerations in mind, the parameters in 4.19 are written as

$$t^L_{\alpha_n}(0_\uparrow) = t_L \langle 1_{\uparrow_{(n)}}| \, b^\dagger_L \, |\emptyset_c\rangle \tag{4.29}$$

$$t^R_{\alpha_n}(0_\uparrow) = t_R \langle \emptyset_c| \, b_R \, |1_{\uparrow_{(n)}}\rangle \tag{4.30}$$

$$t^R_{\beta_m}(0_\uparrow) = 0 \tag{4.31}$$

$$t^L_{\beta_m}(0_\uparrow) = 0 \tag{4.32}$$

$$\epsilon_{\alpha_n}(0_\uparrow) = E_{\alpha_n}(1_\uparrow) \tag{4.33}$$

$$\epsilon_{\beta_m}(0_\uparrow) = 0. \tag{4.34}$$

Equations 4.25, 4.26,4.27 and 4.28 are now written as

$$\begin{cases} \varepsilon_k \psi_0 + \psi_{-1} & = -\sum_n \left(t^L_{\alpha_n(0_\uparrow)}\right)^* \alpha_n \\ (\varepsilon_k - \epsilon_{\alpha_n}(0_\uparrow))\, \alpha_n & = -t^L_{\alpha_n(0_\uparrow)} \psi_0 - \left(t^R_{\alpha_n(0_\uparrow)}\right)^* \psi_{N_c+1} \\ \varepsilon_k \beta_n & = 0 \\ \varepsilon_k \psi_{N_c+1} + \psi_{N_c+2} & = -\sum_n t^R_{\alpha_n(0_\uparrow)} \alpha_n \end{cases} \tag{4.35}$$

From this system of equations, it becomes clear that the transmittance depends on the amplitude of the wavefunction on the left and right contact, $\langle 1_{\uparrow_{(n)}}| \, b^\dagger_L \, |\emptyset_c\rangle$ and $\langle \emptyset_c| \, b_R \, |1_{\uparrow_{(n)}}\rangle$, respectively. It also depends on the energetic difference between the energy of the incoming magnon, ε_k, and the energy separation $E_{\alpha_n} - E_{GS}(0)$. The tunnelling approach makes evident that is not the cluster energy levels per se that matters but the energy difference between levels with $N_\uparrow + 1$ and $N_\uparrow - 1$ and the ground state with $N_\uparrow$.

4.2 Fe^+_{13} cluster magnetic configuration

The magnetic configuration of Fe^+_{13} has been a matter of discussion [31]. While most describe the cluster as ferromagnetic, some claim that the central Fe atom has inverted spin.[31] As an example of the application of the method described in the previous section, the transmittance spectra is computed considering the case where the all sites bonds are ferromagnetic (i.e. its value is $J_{i,j} = J^z_{i,j} > 0$) and where the bonds between external sites are ferromagnetic but anti-ferromagnetic between each external site and the central site (i.e. its value is $J_{i,j} = J^z_{i,j} < 0$). The goal is to compare the behaviour of the incoming magnon for the Fe^+_{13} cluster with ferromagnetic and anti-ferromagnetic couplings and with zero and one magnon within the cluster (corresponding to an inverted central spin).

Table 4.1: Transmittance of a magnon through a Fe_{13}^{+} cluster. The transmittance spectra is computed considering the case where the all sites' bonds are ferromagnetic (i.e. its value is $J_{i,j} = J_{i,j}^{z} > 0$) and where the bonds between external sites are ferromagnetic but anti-ferromagnetic between each external site and the central site (i.e. its value is $J_{i,j} = J_{i,j}^{z} < 0$). The graphics represent the transmittance of incoming magnons with energy ε_k.

	$N_{\uparrow} = 0$	$N_{\uparrow} = 1$
Ferromagnetic 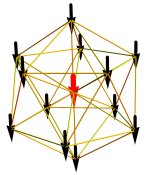	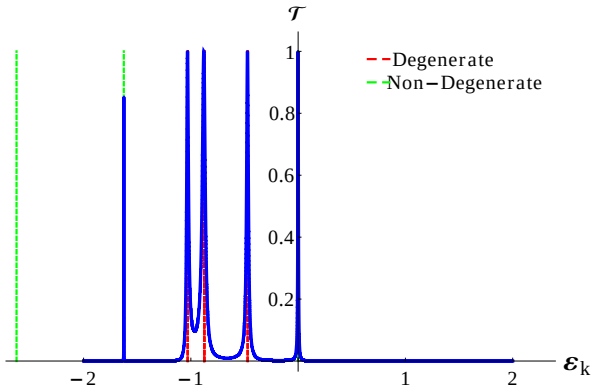	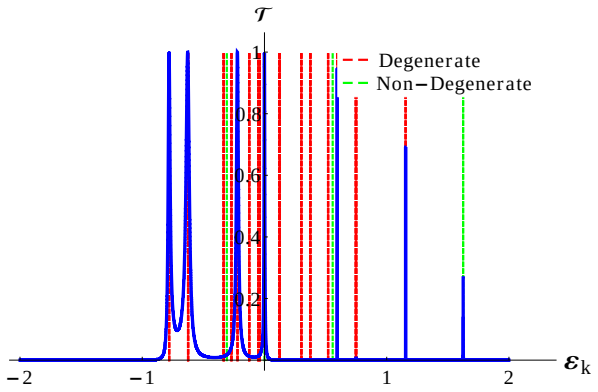
Anti− −ferromagnetic 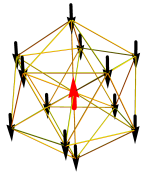	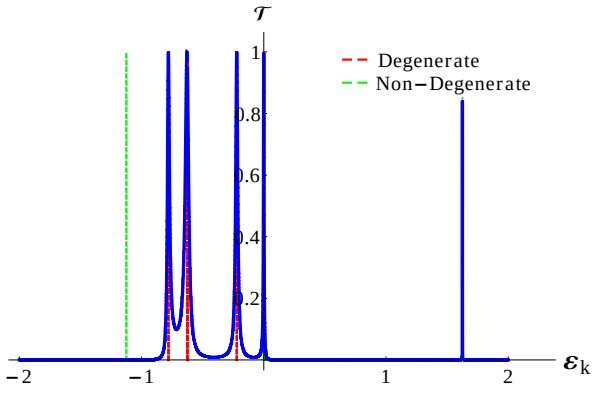	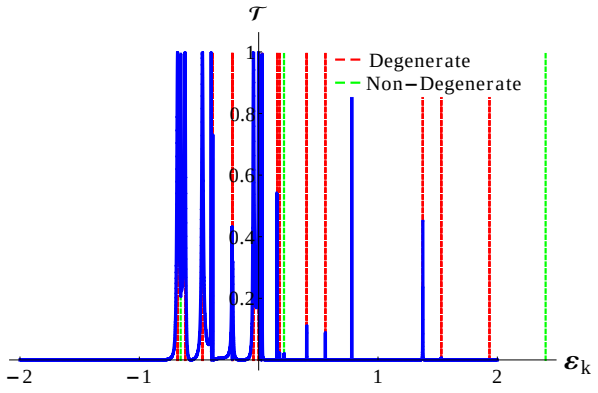

The total magnetic moment of each site was considered to be equal the electron spin magnetic moment $\mu_S \approx \mu_B$, being μ_B the Bohr magneton. Experimental measurements using methods such as chemical probes, [33] photoionization studies, [34]collision-induced dissociation experiments, [35] Stern-Gerlach measurements, [36] photonelectron spectroscopy [30] and time-of-flight mass spectroscopy[37] showed that the total magnetic moment is different than μ_B and it differs from site to site. These Fe_{13}^+ atomic moments do not allow the Matsubara-Matsuda transformation to be considered to compute the transmittance of magnons. Although the Holstein-Primakoff transformation is generalized to sites with spin other than 1/2, it still requires that all sites have equal spin and therefore it also cannot be considered to compute transmittances. The oversimplification of the Fe_{13}^+ cluster means that the results obtained probably do not correspond to the experimental measurements, but may hint on some qualitative conclusions.

Chapter 5

Frustrated magnetic clusters

For some particular geometrically frustrated lattices the existence of localized eigenstates can influence the physics of those systems.[20, 38] The hopping term in the Hamiltonian is responsible for extending a magnon wave function over all lattice sites. The destructive quantum interference phenomena can be responsible for one-magnon eigenfunctions whose amplitudes are only non-zero in restricted areas. These localized magnons have a local character which allows to express many-particle eigenstates of the Hamiltonian as n independent localized magnons even when interactions between magnons are present, given a sufficiently large separation between them.

In this chapter the tunnelling approach developed in the previous chapter is used to compute the transmittance of a single magnon through a frustrated cluster with generalized magnetization. The effects of an external uniform magnetic field in the transmittance is addressed.

5.1 The Saw-tooth Chain

One of the geometries in which localized magnon states arise is the anti-ferromagnetic saw-tooth chain.[39, 40, 41, 42, 43] In this structure there are two types of bonds, J_1 and J_2. The Heisenberg couplings J are considered to be isotropic, that is, $J = J^x = J^y = J^z$ for any given i and j. The eigenstates can be separated in subspaces with different total spin projection $S^z = N_c/2, N_c/2-1, ...$ due to the commutation between S^z and the Hamiltonian. Each subspace has a different number of eigenstates. For $S^z = -N_c/2$ there is only one eigenstate, the fully ferromagnetic state, $|\mathrm{Fe}(\downarrow)\rangle$, which represents the vacuum state for the magnon excitations.

One must calculate the eigenvalues in the one-magnon subspace for the correspondent hard-core Hamiltonian in order to find if a dispersionless one-magnon band can occur. Considering the Hamiltonian given by equation 2.22 in the case of the saw-tooth lattice, we have

$$\begin{aligned} H = \sum_{i=-\infty}^{\infty} \frac{J_1}{2}\left(a_j^\dagger b_j + b_j^\dagger a_j + b_j^\dagger a_{j+1} + a_{j+1}^\dagger b_j\right) + \frac{J_1}{2}\left(a_j^\dagger a_{j+1} + a_{j+1}^\dagger a_j\right) \\ - \left(J_2 + J_1\right) a_j^\dagger a_j - J_2 b_j^\dagger b_j - h\left(a_j^\dagger a_j + b_j^\dagger b_j\right), \end{aligned} \tag{5.1}$$

where $a_j^\dagger$ and $b_j^\dagger$ are the magnon creation operators for positions A_j and B_j and a_j and b_j are the magnon annihilation operators for positions A_j and B_j (See figure 5.1). The two one-

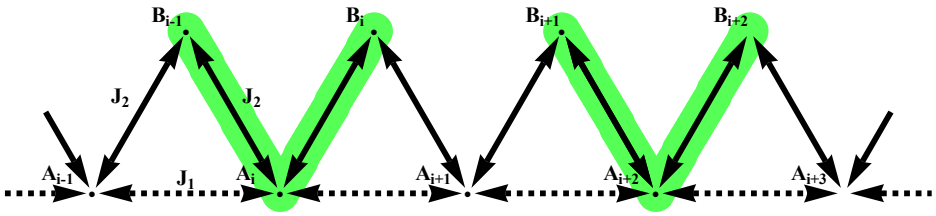

Figure 5.1: Schematic representation of a saw-tooth chain. The Heisenberg coupling between two consecutive sites A is J_1 while the same term between a site A and a site B is J_2. The green shapes represent the localized states. One can see that, when $J_2 = 2J_1 \wedge J_1 < 0 \wedge J_2 < 0$, at most, there is a localized state for every four sites.

---

magnon branches are obtained by going to the momentum space using the Fourier transform

$$a_i = \frac{1}{\sqrt{N_{cells}}} \sum_{\vec{k}} a_{\vec{k}} e^{i\vec{k}.\vec{R}_i^a} \tag{5.2}$$

and

$$b_i = \frac{1}{\sqrt{N_{cells}}} \sum_{\vec{k}} a_{\vec{k}} e^{i\vec{k}.\vec{R}_i^b}. \tag{5.3}$$

Assuming unitary distance between neighbours, one obtains

$$\epsilon_{\pm}(k) = h - \frac{J_1 + 2J_2}{2} + \frac{1}{2}\left[J_1 \cos k \pm \sqrt{J_1^2 \left(\cos k - 1\right)^2 + 2J_2^2 \left(1 + \cos k\right)}\right]. \tag{5.4}$$

If J_1 and J_2 are such that $J_2 = 2J_1$, the lowest magnon branch becomes dispersionless,

$$\epsilon_-(k) = \epsilon_- = h - 4J_1. \tag{5.5}$$

This dispersionless band is associated with the presence of localized excitations of the form

$$|1\rangle = \frac{1}{\sqrt{6}}\left(b_{2j-1}^\dagger - 2a_{2j}^\dagger + a_{2j+1}^\dagger\right)|\mathrm{Fe}(\downarrow)\rangle\,. \tag{5.6}$$

The localized magnons are confined in the valleys as shown in fig 5.1. For these magnons to be independent of each other, each pair of magnons must be separated by at least one empty valley. The maximum number of localized magnons in a saw-tooth chain is then restricted and given by $n_{max} = N_c/4$. The energy of a $N_\uparrow$-localized magnons state is given by

$$E_{N_\uparrow} = E_{\mathrm{Fe}(\downarrow)} + \left(N_\uparrow - \frac{N_c}{2}\right)h - 4J_1 N_\uparrow = E_{\mathrm{Fe}(\downarrow)} - \frac{N_c}{2}h + N_\uparrow(h - 4J_1). \tag{5.7}$$

In order to calculate the magnetization M at $T = 0$ for a given magnetic field, it is only required to find the lowest energy levels $E(M)$ in the subspaces with different $M = N_c/2, N_c/2 - 1, ...$ for zero magnetic field, i.e. $h = 0$. The energies in the presence of an external magnetic field h are given by $E(M, h) = E(M, 0) - hM$. For a given value of h, the magnetization is such that $E(M, h)$ is minimized.

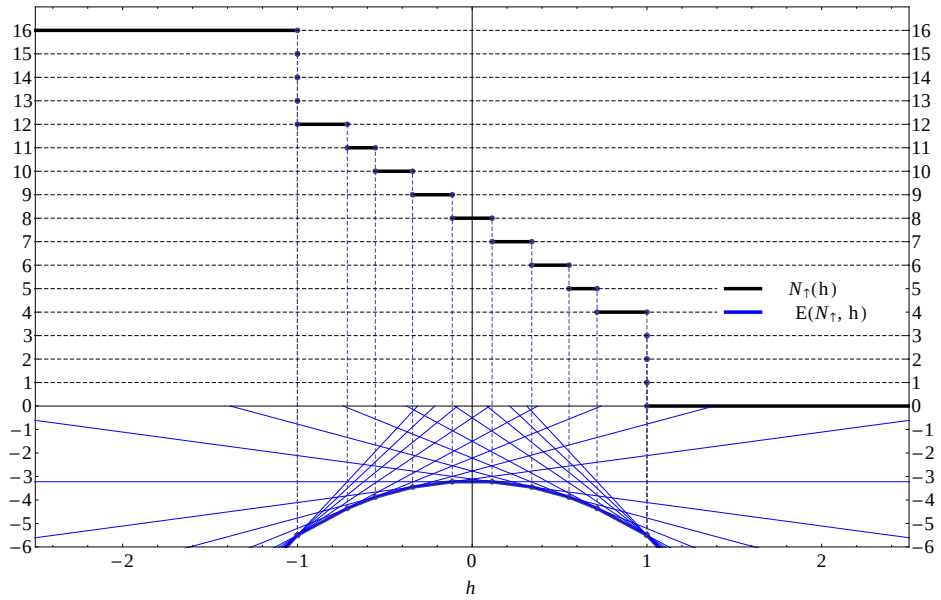

Figure 5.2: Dependency of the number of magnons present in the saw-tooth chain with 16 sites for $\epsilon = 0$, $\epsilon^z = 0$, $\epsilon^z_{\text{Leads}}$, $\epsilon^z_L = \epsilon^z_R = 0$, $J_1 = -0.25$, $J_2 = -0.5$, $J_L = J_R = 0.225$ and $J_{\text{Leads}} = 2$. The energies of the ground state for all possible number of magnons are plotted below. The number of magnons is that of the state with lowest energy for a given magnetic field. The blue dots represent the values of h where the number of magnons present in the cluster changes in order to minimize the cluster energy. Although theses changes add or or subtract a magnon, in frustrated systems these changes can add or subtract more than a magnon. One observes jumps from 0 to 4 and 12 to 16 in the sawtooth chain with 16 sites.

As the magnetic field changes, the magnetization also changes. In classical non-frustrated Heisenberg antiferromagnets, it is common to find the parabolic relation $E(m) \propto M^2$ which leads to $M \propto h$. This linear nature can suffer small deviations due to quantum fluctuations. Systems with frustration and quantum fluctuations can present very distinct curves from the non-frustrated systems. Frustrated magnetic clusters generally present magnetization plateaus.[20, 41] These magnetization plateaus play a fundamental role in the transmittance of magnon waves through the cluster. An external magnetic field determines the magnetization of the cluster which is equivalent to the number of existing magnons in the cluster $N_\uparrow$. As seen in the chapter 4, the transmittance of magnons by tunnelling depends on a set of equations constructed using the energy states for a particular $N_\uparrow$ in the cluster. This means that when $N_\uparrow$ changes due to the magnetic field, the transmittance is ruled by a different set of equations. Moreover, even when the magnetic field is not varied enough to promote a magnetization transition, it always changes the $E(M, h)$. This means that $E_{\mathrm{GS}(N_\uparrow)}$, E_{α_i} and E_{β_n} are changed by the magnetic field thus modifying the transmittance. To understand how the transmittance behaves when the magnetization suddenly changes, the transmittance was computed for a number of magnons in the cluster ranging from 0 to N_c in the presence of a external magnetic field, h (see fig. 5.3). For each value of h, the state with the lowest energy (out of all states with any number of magnons) is selected and the correspondent number of particles is determined. For that h, the value of transmittance is given by the value of transmittance with the number of particles determined previously. Varying h, one obtains a transmittance plot that is given by merging segments of transmittance plots with fixed $N_\uparrow$.

In order to reduce the computing time, a small sized saw-tooth chain (with 7 sites) was chosen. For this reason, the plateaus are not visible.

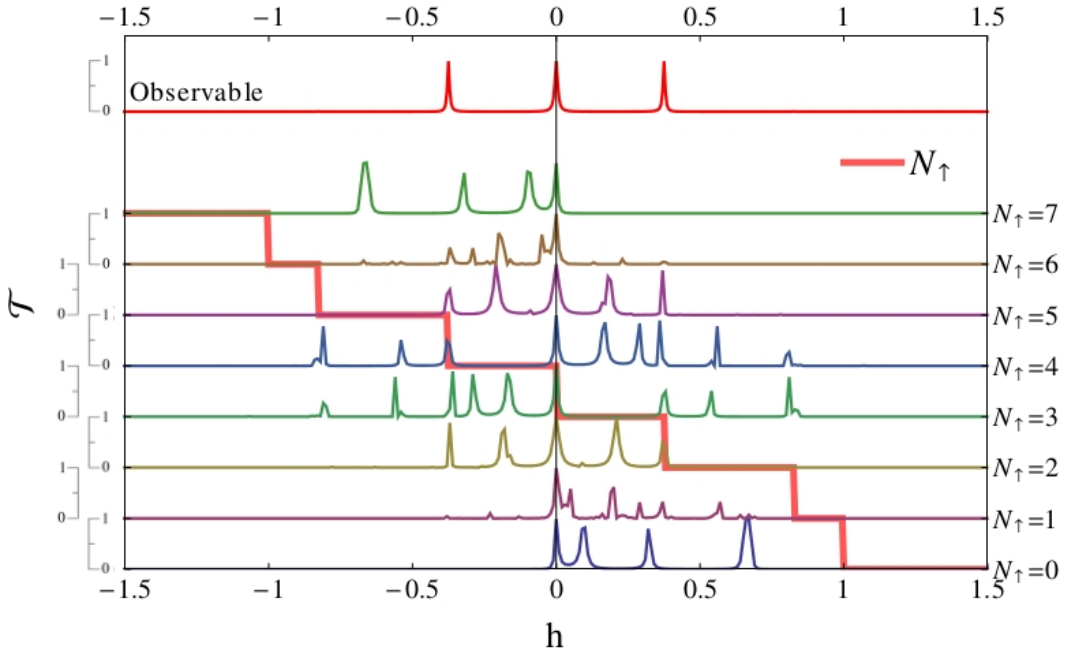

Figure 5.3: Transmittance profiles of magnons with $\varepsilon_k = 0$ for a seven site anti-ferromagnetic saw-tooth chain as functions of the external magnetic field for $\epsilon = 0$, $\epsilon^z = 0$, $\epsilon^z_{\text{Leads}}$, $\epsilon^z_L = \epsilon^z_R = 0$, $J_1 = -0.25$, $J_2 = -0.5$, $J_L = J_R = 0.225$ and $J_{\text{Leads}} = 2$. The transmittance was computed for a number of magnons, $N_\uparrow$, ranging from 0 to N_c. The changes of the number of magnons present in the cluster due to the magnetic field is represented by the pink step function. The observable transmittance is dictated by the number of magnons present for a given magnetic field.

Chapter 6

Conclusion

In this thesis, we have shown that the transport of coherent magnons through mesoscopic magnetic clusters can be modelled by a tunnelling approach even in the case of interaction between magnons.

In the case of ferromagnetic clusters, for transmittance of magnons to occur, the following conditions must be satisfied:

1. The energy of the incoming magnon must be close to the difference between the energy of the ferromagnetic ground state and one of the cluster states with one magnon.

2. The state with energy close to the incoming magnon energy must have finite probability density at both contacts sites.

The transmittance presents sharp peaks at the energies described in chapters 3 and 4 whose width and height depend on t_L and t_R. States with close energies can interfere and the resulting transmittance peak may be different from a simple average of the transmittance peaks. Structures with non-homogeneous coordination number Z_i have effective local potentials which are not present in conventional charge transport. A magnetic tip can be used to alter the transmittance and produce patterns that reflect the probability density profiles of the eigenstates of the cluster.

The tunnelling approach enables to study the transmittance of magnons through clusters with arbitrary magnetization taking into account interactions between magnons. The conditions for transmittance are generalized:

1. The energy of the incoming magnon must be close to the difference between the energy of the ground state with $N_\uparrow$ and one of the states with $N_\uparrow + 1$ up spins or between the energy of the ground state with $N_\uparrow$ up spins and one of the states with $N_\uparrow - 1$.

2. The state with energy close to the incoming magnon's energy depends on the values of $\langle N_\uparrow + 1_{(n)}| \, b_L^\dagger \, |\mathrm{GS}(N_\uparrow)\rangle$, $\langle \mathrm{GS}(N_\uparrow)| \, b_R \, |N_\uparrow + 1_{(n)}\rangle$, $\langle N_\uparrow - 1_{(m)}| \, b_R \, |\mathrm{GS}(N_\uparrow)\rangle$ and $\langle \mathrm{GS}(N_\uparrow)| \, b_L^\dagger \, |N_\uparrow - 1_{(m)}\rangle$.

The number of magnons (inverted spins) present in a cluster is affected by the cluster's structure and the presence of an applied magnetic field. The magnetic field produces magnetization plateaus with transmittance peaks in the magnetization transitions. The observable transmittance is the result of the selection of the transmittance patterns which have the correct magnetization for each magnetic field intensity.

Appendices

Appendix A

Momentum Jordan-Wigner Transformation

To write out the fermionized Hamiltonian obtained in the Jordan-Wigner transformation of the Heisenberg Hamiltonian (eq. 2.38) in a more compact form, a transformation to momentum space is performed

$$f_j = \frac{1}{\sqrt{N}} \sum_k f_k e^{ikR_j}, \tag{A.1}$$

where f_k annihilates a spin excitation with momentum k, N is the number of sites in the 1D chain and R_j is the position of site j. In this case, the fermionized Hamiltonian components become

$$\begin{aligned} J^z \sum_j n_j &= \frac{J^z}{N} \sum_j \left(\sum_{k_1} f_{k_1}^\dagger e^{-ik_1 R_j} \right) \left(\sum_{k_2} f_{k_2} e^{ik_2 R_j} \right) \\ &= J^z \sum_k f_k^\dagger f_k, \end{aligned} \tag{A.2}$$

$$-\frac{J}{2} \sum_j \left(f_{j+1}^\dagger f_j + f_j^\dagger f_{j+1} \right) = -J \sum_k \cos(ka) f_k^\dagger f_k, \tag{A.3}$$

with a constant separation between sites $R_{j+1} - R_j = a$. The second-term of 2.38 can as well be cast to the momentum space

$$J^z \sum_j n_j n_{j+1} = \frac{J^z}{N} \sum_{k_2,k_3,k_4} e^{i(k_4-k_3)a} f_{k_2-k_3+k_4}^\dagger f_{k_2} f_{k_3}^\dagger f_{k_4}. \tag{A.4}$$

Using the following variables exchanges

$$\begin{cases} k - q &= k_2 - k_3 + k_4, \\ k' &= k_3, \\ k &= k_2, \\ k' &= k_4, \end{cases} \tag{A.5}$$

one obtains

$$J^z \sum_j n_j n_{j+1} = \frac{J^z}{N} \sum_{k,k',q} \cos(qa) f^\dagger_{k-q} f^\dagger_{k'+q} f_{k'} f_k. \tag{A.6}$$

Appendix B

Ground State energy for $J^z = 0$

In this appendix, we determine the ground state energy in the XY limit of teh Heisenberg Hamiltonian. Excitations of the ground-state can be made, either by adding a magnon at wavevectors $|k| > \pi/2a$, or by annihilating a magnon at wavevectores $|k| < \pi/2a$, to form a "hole". The energy to form a hole is $-\omega_k$. To better represent the hole excitations, we make a "particle-hole" transformation for the occupied states, writing

$$f_k^\dagger = \begin{cases} \tilde{f}_k^\dagger & , |k| > \pi/2a \\ \tilde{f}_{-k} & , |k| < \pi/2a \end{cases} \tag{B.1}$$

These are the "physical" excitation operators. The Hamiltonian of the pure XY ferromagnet can be written as

$$\begin{aligned} H_{xy} &= -J \sum_k \cos(ka)\, f_k^\dagger f_k \\ &= -J \left(\sum_{|k|<\pi/2a} \cos(ka)\, f_k^\dagger f_k \right) - J \left(\sum_{|k|>\pi/2a} \cos(ka)\, f_k^\dagger f_k \right) \\ &= -J \sum_k |\cos ka| \left(\tilde{f}_k^\dagger \tilde{f}_k - \frac{1}{2} \right). \end{aligned} \tag{B.2}$$

Here the ground state is the state where the magnons occupy the on-particle energy states with absolute momentum lower than $\pi/2a$. Furthermore the number of sites is considered to be very large, allowing to turn the summation into a integral. Using

$$\begin{cases} \sum_k 1 = N \\ \int_{-\pi/2a}^{\pi/2a} \frac{dk}{g} = N \end{cases} \implies N = \frac{2\pi}{ag} \implies g = \frac{2\pi}{Na}, \tag{B.3}$$

the ground state energy is then given by

$$\begin{aligned} E_g =& -J \sum_{|k|<\pi/2a} |\cos(ka)| \\ =& -J \int_{-\pi/2a}^{\pi/2a} \frac{Na}{2\pi} |\cos(ka)| dk \\ =& \frac{JNa}{2\pi} \int_{-\pi/2a}^{\pi/2a} \cos(ka) dk \\ =& \frac{JNa}{2\pi} \left[\frac{-\sin(ka)}{a} \right]_{-\pi/2a}^{\pi/2a} \\ =& \frac{-JN}{\pi}. \end{aligned} \tag{B.4}$$

Appendix C

The 2D Jordan-Wigner Hamiltonian

The Heisenberg Hamiltonian is given by $H = H_{xy} + H_z + H_{\text{Zeeman}}$, with H_{xy} the XY interaction contribution, H_z the Ising interaction term and H_{Zeeman} is the Zeeman effect contribution due to the interaction with an external magnetic field. The Hamiltonian for an infinite 2D lattice can be written as:

$$H = \underbrace{\sum_{i=0}^{\infty}\sum_{j=0}^{\infty} J\left(\mathbf{S}_{i,j}\mathbf{S}_{i+1,j} + \mathbf{S}_{i,j}\mathbf{S}_{i,j+1}\right)}_{H_{xyz}} + \underbrace{\sum_{i=0}^{\infty}\sum_{j=0}^{\infty} hS_{i,j}^{z}}_{H_f} \tag{C.1}$$

Using the extended Jordan-Wigner transformation, one can separate the XY interaction from the z interaction, and we have

$$\begin{aligned}
H_{xy} &= \sum_{i=0}^{\infty}\sum_{j=0}^{\infty} \frac{1}{2}J_{i,j,i+1,j}\left(S_{i,j}^{+}S_{i+1,j}^{-} + S_{i,j}^{-}S_{i+1,j}^{+}\right) + \frac{1}{2}J_{i,j,i,j+1}\left(S_{i,j}^{+}S_{i,j+1}^{-} + S_{i,j}^{-}S_{i,j+1}^{+}\right) \\
&= \frac{1}{2}\sum_{i=0}^{\infty}\sum_{j=0}^{\infty} J_{i,j,i+1,j} f_{i,j}^{\dagger} e^{-i\pi\left(\sum_{d=0}^{i-1}\sum_{w=0}^{\infty} n_{d,w} + \sum_{w=0}^{j-1} n_{i,w}\right)} f_{i+1,j} e^{i\pi\left(\sum_{d=0}^{i}\sum_{w=0}^{\infty} n_{d,w} + \sum_{w=0}^{j-1} n_{i,w}\right)} \\
&+ J_{i,j,i+1,j} f_{i,j} e^{i\pi\left(\sum_{d=0}^{i-1}\sum_{w=0}^{\infty} n_{d,w} + \sum_{w=0}^{j-1} n_{i,w}\right)} f_{i+1,j}^{\dagger} e^{-i\pi\left(\sum_{d=0}^{i}\sum_{w=0}^{\infty} n_{d,w} + \sum_{w=0}^{j-1} n_{i,w}\right)} \\
&+ J_{i,j,i,j+1}\left(f_{i,j}^{\dagger} e^{i\pi n_{i,j}} f_{i,j+1} + f_{i,j} e^{-i\pi n_{i,j}} f_{i,j+1}^{\dagger}\right) \\
&= \frac{1}{2}\sum_{i=0}^{\infty}\sum_{j=0}^{\infty} J_{i,j,i+1,j} f_{i,j}^{\dagger} e^{i\pi\left(\sum_{w=j+1}^{\infty} n_{i,w} + \sum_{w=0}^{j-1} n_{i+1,w}\right)} f_{i+1,j} \\
&- J_{i,j,i+1,j} f_{i,j} e^{-i\pi\left(\sum_{w=j+1}^{\infty} n_{i,w} + \sum_{w=0}^{j-1} n_{i+1,w}\right)} f_{i+1,j}^{\dagger} \\
&+ J_{i,j,i,j+1}\left(f_{i,j}^{\dagger} f_{i,j+1} - f_{i,j} f_{i,j+1}^{\dagger}\right)
\end{aligned} \tag{C.2}$$

Replacing $\pi\left(\sum_{w=j+1}^{\infty} n_{i,w} + \sum_{w=0}^{j-1} n_{i+1,w}\right)$ by $\tilde{\phi}_{i,i+1}(j)$, we obtain

$$\begin{aligned} H_{xy} = \frac{1}{2}\sum_{i=0}^{\infty}\sum_{j=0}^{\infty} J_{i,j,i+1,j}\left(-f_{i,j}e^{i\tilde{\phi}_{i,i+1}(j)}f_{i+1,j}^{\dagger} + f_{i,j}^{\dagger}e^{-i\tilde{\phi}_{i,i+1}(j)}f_{i+1,j}\right) \\ + J_{i,j,i,j+1}\left(-f_{i,j}f_{i,j+1}^{\dagger} + f_{i,j}^{\dagger}f_{i,j+1}\right). \end{aligned} \tag{C.3}$$

This can be viewed as the Hamiltonian of a two-dimensional tight-binding-like spinless fermionic Hamiltonian with the hopping amplitudes

$$\begin{cases} \pm\frac{1}{2}J_{i,j,i+1,j}e^{\pm i\tilde{\phi}_{i,i+1}(j)} & \text{, in the x direction} \\ \pm\frac{1}{2}J_{i,j,i,j+1} & \text{, in the y direction.} \end{cases} \tag{C.4}$$

Those hoppings depend in a complicated way on the configuration of the intermediate sites. This complexity explains how the isotropic XY Hamiltonian becomes difficult to examine in two dimensions in comparison with an obvious analysis in one dimension. There are no difficulties in rewriting the Ising interaction in fermionic language

$$\begin{aligned} H_z = \sum_{i=0}^{\infty}\sum_{j=0}^{\infty} J_{i,j,i+1,j}\left(S_{i,j}^{+}S_{i,j}^{-} - \frac{1}{2}\right)\left(S_{i+1,j}^{+}S_{i+1,j}^{-} - \frac{1}{2}\right) \\ + J_{i,j,i,j+1}\left(S_{i,j}^{+}S_{i,j}^{-} - \frac{1}{2}\right)\left(S_{i,j+1}^{+}S_{i,j+1}^{-} - \frac{1}{2}\right) \end{aligned} \tag{C.5}$$

$$\begin{aligned} H_z = \sum_{i=0}^{\infty}\sum_{j=0}^{\infty} J_{i,j,i+1,j}\left(f_{i,j}^{\dagger}f_{i,j} - \frac{1}{2}\right)\left(f_{i+1,j}^{\dagger}f_{i+1,j} - \frac{1}{2}\right) \\ + J_{i,j,i,j+1}\left(f_{i,j}^{\dagger}f_{i,j} - \frac{1}{2}\right)\left(f_{i,j+1}^{\dagger}f_{i,j+1} - \frac{1}{2}\right) \end{aligned} \tag{C.6}$$

and the Zeeman interaction due to an external magnetic field

$$H_{\text{Zeeman}} = \sum_{i=0}^{\infty}\sum_{j=0}^{\infty} h\left(S_{i,j}^{+}S_{i,j}^{-} - \frac{1}{2}\right) = \sum_{i=0}^{\infty}\sum_{j=0}^{\infty} h\left(f_{i,j}^{\dagger}f_{i,j} - \frac{1}{2}\right) \tag{C.7}$$

H_{xy}, H_z, H_{Zeeman} realize the fermionic representation of the spin-$\frac{1}{2}$ isotropic Heisenberg model on a square lattice.

Bibliography

[1] Robert L Stamps et al., "The 2014 Magnetism Roadmap", in: *Journal of Physics D: Applied Physics* 47.33 (2014).

[2] C. W. Sandweg et al., "Spin Pumping by Parametrically Excited Exchange Magnons", in: *Phys. Rev. Lett.* 106 (21 May 2011).

[3] Varlei Rodrigues et al., "Evidence for Spontaneous Spin-Polarized Transport in Magnetic Nanowires", in: *Phys. Rev. Lett.* 91 (9 Aug. 2003).

[4] Alexander Khitun, Mingqiang Bao, and Kang L Wang, "Magnonic logic circuits", in: *Journal of Physics D: Applied Physics* 43.26 (July 2010).

[5] Xufeng Zhang et al., "Electric-Field Coupling to Spin Waves in a Centrosymmetric Ferrite", in: *Phys. Rev. Lett.* 113 (3 July 2014), p. 037202.

[6] Y. Tserkovnyak, A. Brataas, and G. E. Bauer, "Enhanced Gilbert Damping in Thin Ferromagnetic Films", in: *Physical Review Letters* 88.11 (Mar. 2002).

[7] K. Nakata, "Quantum Spin Pumping Mediated by Magnon", in: *Journal of the Physical Society of Japan* 81.6 (June 2012).

[8] Gerrit E. Bauer and Yaroslav Tserkovnyak, "Spin-magnon transmutation", in: *Physics* 4 (May 2011).

[9] Haiming Yu et al., "Omnidirectional spin-wave nanograting coupler", in: *Nat Comms* 4 (Nov. 2013).

[10] A. A. Serga et al., "Brillouin light scattering spectroscopy of parametrically excited dipole-exchange magnons", in: *Physical Review B* 86.13 (Oct. 2012).

[11] D J Lockwood et al., "Raman scattering from one-magnon excitations in FeF_2", in: *Journal of Physics C: Solid State Physics* 17.33 (1984).

[12] Luuk J. P. Ament et al., "Resonant inelastic x-ray scattering studies of elementary excitations", in: *Reviews of Modern Physics* 83.2 (June 2011).

[13] T. Wolfram and S. Ellialtioglu, "Neutron Scattering by Magnons of an Antiferromagnet with Modulated Spin Amplitudes", in: *Phys. Rev. Lett.* 44 (19 May 1980).

[14] Per-Anker Lindgård, A. Kowalska, and Peter Laut, "Investigation of magnon dispersion relations and neutron scattering cross section with special attention to anisotropy effects", in: *Solid State Communications* 5.2 (1967).

[15] M. Hofmann et al., "Measurements of the polarization of field emitted electrons from polycrystalline gadolinium", in: *Physics Letters A* 25.3 (Aug. 1967).

[16] T. J. Matcovich et al., "Ferromagnetic Resonance Magnon Distribution in Yttrium Iron Garnet", in: *Proceedings of the Seventh Conference on Magnetism and Magnetic Materials*, Springer US, 1962.

[17] J. R. Sandercock, W. Jantz, and W. Wettling, "Magnon dispersion of iron borate studied by light scattering and ferromagnetic resonance", in: *Physica B+C* 89 (1977).

[18] B A Z António, A A Lopes, and R G Dias, "Transport through quantum rings", in: *Eur. J. Phys.* 34.4 (July 2013).

[19] Gerald D. Mahan, *Many-Particle Physics*, 2nd, New York, N.Y.: Plenum, 1993.

[20] C. Lacroix, P. Mendels, and F. Mila, *Introduction to Frustrated Magnetism: Materials, Experiments, Theory*, Springer Series in Solid-State Sciences, Springer, 2011.

[21] O. Derzhko, "Jordan-Wigner fermionization for spin-1/2 systems in two dimensions: A brief review", in: *Journal of Physical Studies* 5 (2001).

[22] T. Schultz, D. Mattis, and E. Lieb, "Two-Dimensional Ising Model as a Soluble Problem of Many Fermions", in: *Reviews of Modern Physics* 36.3 (July 1964).

[23] P. Coleman, *Introduction to many body physics*, Cambridge University Press, 2013.

[24] Mohamed Azzouz, "Interchain-coupling effect on the one-dimensional spin-1/2 antiferromagnetic Heisenberg model", in: *Physical Review B* 48.9 (Sept. 1993).

[25] T. Holstein and H. Primakoff, "Field Dependence of the Intrinsic Domain Magnetization of a Ferromagnet", in: *Phys. Rev.* 58 (12 Dec. 1940).

[26] C. Kittel, *Quantum Theory of Solids*, Wiley, 1963.

[27] Olaf Strelcyk, Thomas Korb, and Herbert Schoeller, "Magnon transport and spin current switching through quantum dots", in: *Physical Review B* 72.16 (Oct. 2005).

[28] Frank Reininghaus, Thomas Korb, and Herbert Schoeller, "Fingerprints of the Magnetic Polaron in Nonequilibrium Electron Transport through a Quantum Wire Coupled to a Ferromagnetic Spin Chain", in: *Phys. Rev. Lett.* 97.2 (July 2006).

[29] M. Niemeyer et al., "Spin Coupling and Orbital Angular Momentum Quenching in Free Iron Clusters", in: *Phys. Rev. Lett.* 108 (5 Jan. 2012), p. 057201.

[30] Lai-Sheng Wang, Han-Song Cheng, and Jiawen Fan, "Photoelectron spectroscopy of size-selected transition metal clusters: Fe_n, $n = 3 - 24$", in: *J. Chem. Phys.* 102.24 (1995).

[31] O. Dieguez et al., "Density-functional calculations of the structures, binding energies, and magnetic moments of Fe clusters with 2 to 17 atoms", in: *Physical Review B* 63.20 (Apr. 2001).

[32] A. A. Lopes and R. G. Dias, "Simple approach for the two-terminal conductance through interacting clusters", in: *ArXiv e-prints* (July 2014).

[33] E. K. Parks et al., "Chemical probes of metal cluster structure: Reactions of iron clusters with hydrogen, ammonia, and water", in: *J. Chem. Phys.* 88.3 (1988).

[34] Shihe Yang and Mark B. Knickelbein, "Photoionization studies of transition metal clusters: Ionization potentials for Fe_n and Co_n", in: *J. Chem. Phys.* 93.3 (1990).

[35] Li Lian, C.-X. Su, and P. B. Armentrout, "Collision-induced dissociation of Fe_n^+ ($n = 2 - 19$) with Xe: Bond energies, geometric structures, and dissociation pathways", in: *J. Chem. Phys.* 97.6 (1992).

[36] D. Cox et al., "Magnetic behavior of free-iron and iron oxide clusters", in: *Physical Review B* 32.11 (Dec. 1985).

[37] Masaki Sakurai et al., "Magic numbers in transition metal (Fe, Ti, Zr, Nb, and Ta) clusters observed by time-of-flight mass spectrometry", in: *J. Chem. Phys.* 111.1 (1999).

[38] J. Richter, "Localized-magnon states in strongly frustrated quantum spin lattices", in: *Low Temp. Phys.* 31.8 (2005).

[39] Tota Nakamura and Kenn Kubo, "Elementary excitations in the Delta chain", in: *Physical Review B* 53.10 (Mar. 1996).

[40] D. Sen et al., "Quantum solitons in the sawtooth lattice", in: *Physical Review B* 53.10 (Mar. 1996).

[41] J. Richter et al., "Exact eigenstates and macroscopic magnetization jumps in strongly frustrated spin lattices", in: *Journal of Physics: Condensed Matter* 16.11 (Mar. 2004).

[42] Claudine Lacroix, Philippe Mendels, and Frédéric Mila, eds., *Introduction to Frustrated Magnetism*, Springer Berlin Heidelberg, 2011.

[43] J. Ritcher, O. Derzho, and A. Honecker, "The Sawtooth Chain: From Heinsenberg spins to Hubbard electrons", in: *Int. J. Mod. Phys. B* 22.25n26 (Oct. 2008).